

Stabilization of High Order Cut Finite Element Methods on Surfaces*

Mats G. Larson [†] Sara Zahedi [‡]

Abstract

We develop and analyze a stabilization term for cut finite element approximations of an elliptic second order partial differential equation on a surface embedded in \mathbb{R}^d . The new stabilization term combines properly scaled normal derivatives at the surface together with control of the jump in the normal derivatives across faces and provides control of the variation of the finite element solution on the active three dimensional elements that intersect the surface. We show that the condition number of the stiffness matrix is $O(h^{-2})$, where h is the mesh parameter. The stabilization term works for linear as well as for higher-order elements and the derivation of its stabilizing properties is quite straightforward, which we illustrate by discussing the extension of the analysis to general n -dimensional smooth manifolds embedded in \mathbb{R}^d , with codimension $d - n$. We also formulate properties of a general stabilization term that are sufficient to prove optimal scaling of the condition number and optimal error estimates in energy- and L^2 -norm. We finally present numerical studies confirming our theoretical results.

1 Introduction

CutFEM for Surface Partial Differential Equations. CutFEM (Cut Finite Element Method) provides a new high order finite element method for solution of partial differential equations on surfaces. The main approach is to embed the surface into a three dimensional mesh and to use the restriction of the finite element functions to the surface as trial and test functions. More precisely, let Γ be a smooth closed surface embedded in \mathbb{R}^3 with exterior unit normal n and consider the Laplace-Beltrami problem: find $u \in H^1(\Gamma)$ such that

$$a(u, v) = l(v) \quad \forall v \in H^1(\Gamma). \quad (1.1)$$

The forms are defined by

$$a(w, v) = \int_{\Gamma} \nabla_{\Gamma} w \cdot \nabla_{\Gamma} v, \quad l(v) = \int_{\Gamma} f v, \quad (1.2)$$

where ∇_{Γ} is the surface gradient and $f \in L^2(\Gamma)$ a given function with average zero. Let now Γ be embedded into a polygonal domain Ω equipped with a quasi-uniform mesh $\mathcal{T}_{h,0}$ and let

*This research was supported in part by the Swedish Foundation for Strategic Research Grant No. AM13-0029, the Swedish Research Council Grants Nos. 2013-4708 and 2014-4804, and the Swedish Research Programme Essence

[†]Department of Mathematics and Mathematical Statistics, Umeå University, SE-90187 Umeå, Sweden

[‡]Department of Mathematics, KTH Royal Institute of Technology, SE-100 44 Stockholm, Sweden

Γ_h be a family of discrete surfaces that converges to Γ in an appropriate manner. Let the active mesh \mathcal{T}_h consist of all elements that intersect Γ_h . Let V_h be the space of continuous piecewise polynomial functions on \mathcal{T}_h with average zero on Γ_h . The basic CutFEM takes the form: find $u_h \in V_h$ such that

$$a_h(u_h, v) = l_h(v) \quad \forall v \in V_h, \quad (1.3)$$

where

$$a_h(w, v) = \int_{\Gamma_h} \nabla_{\Gamma} w \cdot \nabla_{\Gamma} v, \quad l_h(v) = \int_{\Gamma_h} f_h v, \quad (1.4)$$

and f_h is a suitable representation of f on Γ_h . In the context of surface partial differential equations this approach, also called trace finite elements, was first introduced in [26] and has then been developed in different directions including high order approximations in [29], discontinuous Galerkin methods [6], transport problems [28], embedded membranes [12], coupled bulk-surface problems [8] and [19], minimal surface problems [11], and time dependent problems on evolving surfaces [23], [25], [27], and [30]. We also refer to the overview article [2] and the references therein.

Previous Work on Preconditioning and Stabilization. The basic CutFEM method (1.3) manufactures a potentially ill conditioned linear system of equations and stabilization or preconditioning is therefore needed. In [24] it was shown that diagonal preconditioning works for piecewise linear approximation and in [29] it was shown that also quadratic elements can be preconditioned if the full gradient is used instead of the tangential gradient in the bilinear form a_h , see also [13] where this formulation was proposed.

In [3] a stabilized version of (1.3) was introduced. The method takes the form

$$a_h(u_h, v) + s_h(u_h, v) = l(v) \quad \forall v \in V_h, \quad (1.5)$$

where s_h is a stabilization form which is added in order to ensure stability of the method. More precisely we show that there is a constant such that for all $v \in V_h$,

$$\|v\|_{L^2(\mathcal{T}_h)}^2 \lesssim h(a_h(v, v) + s_h(v, v)). \quad (1.6)$$

Using (1.6) and the properties of a_h we can show that the condition number κ of the stiffness matrix satisfies the optimal bound

$$\kappa \lesssim h^{-2}. \quad (1.7)$$

In [3] only piecewise linear finite elements were considered and the stabilization term was defined by

$$s_h(w, v) = c_F([D_{n_F}^1 w], [D_{n_F}^1 v])_{\mathcal{F}_h}, \quad (1.8)$$

where $[D_{n_F}^1 v]$ is the jump in the normal derivative of v at the face F , \mathcal{F}_h is the set of internal faces (i.e. faces with two neighbors) in the active mesh \mathcal{T}_h , and $c_F > 0$ is a stabilization parameter. Optimal order bounds on the error and condition number were established. Furthermore, for linear elements the so called full gradient stabilization

$$s_h(v, w) = ch(\nabla v, \nabla w)_{\mathcal{T}_h} \quad (1.9)$$

was proposed and analyzed in [7] as a simpler alternative, and for higher order elements the normal gradient stabilization

$$s_h(w, v) = c_{\mathcal{T}} h^\alpha (n_h \cdot \nabla w, n_h \cdot \nabla v)_{\mathcal{T}_h}, \quad \alpha \in [-1, 1], \quad (1.10)$$

was proposed and analysed independently in [5] and [18]. The restrictions on α essentially comes from a lower bound which implies that optimal order a priori error estimates hold and an upper bound which implies that the desired stability estimate (1.6) holds. Note that stronger control than (1.6) is sometimes demanded, for instance in cut discontinuous Galerkin methods [6], which may lead to stronger upper restrictions on α .

The last two stabilization terms, (1.9) and (1.10), can however not be used in the discretization of bulk problems without destroying the convergence order while the ghost penalty stabilization term [10], which as (1.8) acts on the element faces, can be used. Thus, in many applications where both bulk and surface problems occur face stabilization is still needed when discretizing the problem with CutFEM. It should be noted that the stabilization term (1.8) has been used also for other reasons than controlling the condition number. It is used for example in [9] to stabilize for convection and in [22] to improve on the accuracy of computing the mean curvature vector of a surface. We study the problem of computing the mean curvature vector of a surface based on the Laplace-Beltrami operator in Section 9.3.

New Contributions. In this work we consider stabilization for linear as well as higher-order elements using a combination of face stabilization and normal derivative stabilization at the actual surface. More precisely the stabilization term takes the form

$$s_h(v, w) = s_{h,F}(v, w) + s_{h,\Gamma}(v, w) \quad (1.11)$$

with

$$s_{h,F}(v, w) = \sum_{j=1}^p c_{F,j} h^{2(j-1+\gamma)} ([D_{n_F}^j v], [D_{n_F}^j w])_{\mathcal{F}_h}, \quad (1.12)$$

$$s_{h,\Gamma}(v, w) = \sum_{j=1}^p c_{\Gamma,j} h^{2(j-1+\gamma)} (D_{n_h}^j v, D_{n_h}^j w)_{\Gamma_h}, \quad (1.13)$$

where $\gamma \in [0, 1]$ is a parameter, $[D_{n_F}^j v]$ is the jump in the normal derivative of order j across the face F , and $c_{F,j} > 0$, $c_{\Gamma,j} > 0$, are stabilization constants. This stabilization term with $\gamma = 1$ has also been used in a high order space-time CutFEM on evolving surfaces [30]. We note that also for this stabilization term there is a certain range of scaling with the mesh parameter h , and in fact the following stronger version of (1.6) holds for $v \in V_h$

$$\|v\|_{L^2(\mathcal{T}_h)}^2 + h^{2\gamma} \|\nabla v\|_{L^2(\mathcal{T}_h)}^2 \lesssim h(a_h(v, v) + s_h(v, v)), \quad (1.14)$$

where we get stronger control of the gradient for smaller $\gamma \in [0, 1]$, which corresponds to stronger stabilization.

Using the combination of the face and surface stabilization terms the proof of (1.6) consists of two steps:

- Using the face terms we can estimate the L^2 norm of a finite element function at an element in terms of the L^2 norm at a neighboring element which share a face and the stabilization term on the shared face. Repeating this procedure we can pass from any element to an element which has a large intersection, $|T \cap \Gamma_h| \gtrsim h^2$, with Γ_h .

- Using the stabilization of normal derivatives at the surface we can control a finite element function on elements which have large intersection with Γ_h .

Using shape regularity we can show that one can pass from any element in \mathcal{T}_h to an element with a large intersection in a uniformly bounded number of steps, see [3] and [15]. The analysis is quite straight forward and may in fact also be extended to the case on an n -dimensional smooth manifold embedded in \mathbb{R}^d for general codimension $cd = d - n$. An important special case is a curve embedded in \mathbb{R}^3 , which may for instance be an intersection of two surfaces, see also [4] for generalizations to so called mixed dimensional problems. For clarity, we consider a two dimensional surface embedded in \mathbb{R}^3 throughout the paper and discuss the minor modifications necessary in a separate section. We also refer to [5] for general background on the analysis of problems with higher codimension embeddings.

Outline. In Section 2 we introduce the model problem, in Section 3 we formulate the finite element method, in Section 4 we collect some basic preliminary results, in Section 5 we formulate the properties of the stabilization term, in Section 6 we establish an optimal order condition number estimate, in Section 7 we discuss the extension to problems on n -dimensional smooth manifolds embedded in \mathbb{R}^d , in Section 8 we prove optimal order a priori error estimates, and in Section 9 we present numerical results that support our theoretical findings. In the last section, Section 10, we conclude and discuss the advantages with the proposed stabilization.

2 The Laplace–Beltrami Problem on a Surface

The Surface. Let Γ be a smooth, closed, simply connected surface in \mathbb{R}^3 with exterior unit normal n embedded in a polygonal domain $\Omega \subset \mathbb{R}^3$. Let $U_\delta(\Gamma)$ be the open tubular neighborhood of Γ with thickness $\delta > 0$,

$$U_\delta(\Gamma) = \{x \in \mathbb{R}^3 : |d(x)| < \delta\}, \quad (2.1)$$

where $d(x)$ is the signed distance function of Γ with $d < 0$ in the interior of Γ and $d > 0$ in the exterior. Note that $n = \nabla d$ is the outward-pointing unit normal on Γ . Then there is $\delta_0 > 0$ such that for each $x \in U_{\delta_0}(\Gamma)$ the closest point projection:

$$p(x) = x - d(x)n(p(x)) \quad (2.2)$$

maps x to a unique closest point on Γ . In particular, we require

$$\delta_0 \max_{i=1,2} \|\kappa_i\|_{L^\infty(\Gamma)} < 1, \quad (2.3)$$

where for $x \in \Gamma$, κ_i are the principal curvatures. We also define the extension of a function u on Γ to $U_{\delta_0}(\Gamma)$ by

$$u^e(x) = u(p(x)), \quad x \in U_{\delta_0}(\Gamma). \quad (2.4)$$

The Problem. We consider the problem: find $u \in H_0^1(\Gamma) = \{v \in H^1(\Gamma) \mid \int_\Gamma v \, ds = 0\}$ such that

$$a(u, v) = l(v) \quad \forall v \in H_0^1(\Gamma), \quad (2.5)$$

where

$$a(u, v) = \int_{\Gamma} \nabla_{\Gamma} u \cdot \nabla_{\Gamma} v \, ds, \quad l(v) = \int_{\Gamma} f v \, ds. \quad (2.6)$$

Here ∇_{Γ} is the tangential gradient on Γ defined by

$$\nabla_{\Gamma} u = P_{\Gamma} \nabla u^e, \quad (2.7)$$

where

$$P_{\Gamma} = I - n \otimes n. \quad (2.8)$$

We used the extension of u which is constant in the normal direction to Γ to formally define $\nabla_{\Gamma} u$. However, the tangential derivative depends only on the values of u on Γ and does not depend on the particular choice of extension.

Using Lax-Milgram's Lemma we conclude that there is a unique solution to (2.5), and we also have the elliptic regularity estimate

$$\|u\|_{H^{s+2}(\Gamma)} \lesssim \|f\|_{H^s(\Gamma)}, \quad s \in \mathbb{Z}, \quad s \geq -1. \quad (2.9)$$

3 The Method

3.1 The Mesh and Finite Element Space

- *The background mesh and space:* Let $\mathcal{T}_{h,0}$ be a quasi-uniform partition of Ω with mesh parameter $h \in (0, h_0]$ into shape regular tetrahedra. On $\mathcal{T}_{h,0}$ we define $V_{h,0}^p$ to be the space of continuous piecewise polynomials of degree $p \geq 1$.
- *The discrete surfaces:* Let Γ_h be a sequence of surfaces that converges to Γ . We specify the precise assumptions on the convergence below.
- *The active mesh and the induced surface mesh:* We denote by \mathcal{T}_h the set consisting of elements in the background mesh $\mathcal{T}_{h,0}$ that are cut by the discrete geometry Γ_h . These elements form the so called active mesh. See Fig. 1 for an illustration. The restriction of the active mesh to the discrete surface Γ_h manufactures an induced cut surface mesh that we denote by

$$\mathcal{K}_h = \{K = T \cap \Gamma_h : T \in \mathcal{T}_h\}. \quad (3.1)$$

- *The finite element space:* The restriction of the background space to the active mesh together with the condition $\int_{\Gamma_h} v \, ds_h = 0$ defines our finite element space V_h^p ,

$$V_h^p = \left\{ v_h \in V_{h,0}^p|_{\mathcal{T}_h} : \int_{\Gamma_h} v \, ds_h = 0 \right\}. \quad (3.2)$$

3.2 The Finite Element Method

Method. Find $u_h \in V_h^p$ such that

$$A_h(u_h, v) := a_h(u_h, v) + s_h(u_h, v) = l_h(v) \quad \forall v_h \in V_h^p. \quad (3.3)$$

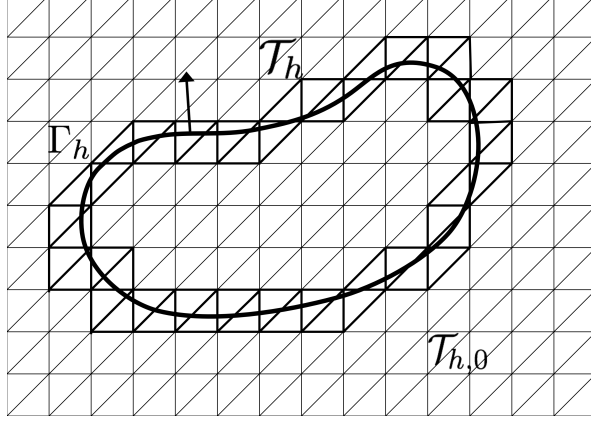


Figure 1: The discrete surface Γ_h , the background mesh $\mathcal{T}_{h,0}$, and the active mesh \mathcal{T}_h .

Forms.

- The forms a_h and l_h are defined by

$$a_h(w, v) = (\nabla_{\Gamma_h} w, \nabla_{\Gamma_h} v)_{\Gamma_h}, \quad l_h(v) = (f_h, v)_{\Gamma_h}, \quad (3.4)$$

where the tangential gradient ∇_{Γ_h} is defined by

$$\nabla_{\Gamma_h} u_h = P_{\Gamma_h} \nabla u_h \quad (3.5)$$

with

$$P_{\Gamma_h} = I - n_h \otimes n_h. \quad (3.6)$$

- The stabilization form s_h is defined by

$$s_h(w, v) = s_{h,F}(w, v) + s_{h,\Gamma}(w, v), \quad (3.7)$$

where

$$s_{h,F}(w, v) = \sum_{j=1}^p c_{F,j} h^{2(j-1+\gamma)} ([D_{n_F}^j w], [D_{n_F}^j v])_{\mathcal{F}_h}, \quad (3.8)$$

$$s_{h,\Gamma}(w, v) = \sum_{j=1}^p c_{\Gamma,j} h^{2(j-1+\gamma)} (D_{n_h}^j w, D_{n_h}^j v)_{\mathcal{K}_h}. \quad (3.9)$$

Here $(D_a^j v)|_x$ is the j -th directional derivative of v along the line defined by the unit vector $a(x)$, $[w]_F$ denotes the jump of w over the face F , \mathcal{F}_h is the set of internal faces (i.e. faces with two neighbors) in the active mesh \mathcal{T}_h , $c_{\Gamma,j} > 0$, $c_{F,j} > 0$ are stabilization parameters, and $\gamma \in [0, 1]$ is a parameter.

Remark 3.1 *In the special case $p = 1$ we obtain*

$$s_h(w, v) = c_F h^{2\gamma} ([D_{n_F}^1 w], [D_{n_F}^1 v])_{\mathcal{F}_h} + c_{\Gamma} h^{2\gamma} (D_{n_h}^1 w, D_{n_h}^1 v)_{\mathcal{K}_h}, \quad (3.10)$$

where $\gamma \in [0, 1]$ which can be compared with the pure face penalty term

$$s_h(w, v) = c_F([D_{n_F}^1 w], [D_{n_F}^1 v])_{\mathcal{F}_h} \quad (3.11)$$

developed in [3]. Note that the scalings with the mesh parameter h are different in the two terms and that for $\gamma > 0$ the face penalty term is weaker in the stabilization term we introduce here.

3.3 Assumptions

A1. We assume that the closed, simply connected approximation Γ_h and its unit normal n_h are such that for all $h \in (0, h_0]$,

$$\|d\|_{L^\infty(\Gamma_h)} \lesssim h^{p+1}, \quad (3.12)$$

$$\|n - n_h\|_{L^\infty(\Gamma_h)} \lesssim h^p, \quad (3.13)$$

that $n \cdot n_h > 0$ on Γ_h , and that we have a uniform bound on the curvature κ_h .

A2. We assume that the mesh is sufficiently small so that there is a constant c independent of the mesh size h such that $\mathcal{T}_h \subset U_\delta(\Gamma)$ with $\delta = ch \leq \delta_0$ and that the closest point mapping $p(x) : \Gamma_h \rightarrow \Gamma$ is a bijection.

A3. We assume that the data approximation f_h is such that $\| |B| f^e - f_h \|_{L^2(\Gamma_h)} \lesssim h^{p+1} \|f\|_{L^2(\Gamma)}$. Here $ds = |B| ds_h$ (see Section 4 for details).

4 Preliminary Results

4.1 Norms

Given a positive semidefinite bilinear form b we let $\|v\|_b^2 = b(v, v)$ denote the associated seminorm. In particular, we will use the following norms on $V_h^p + H^{p+1}(\mathcal{T}_h)$,

$$\|v\|_{a_h}^2 = a_h(v, v), \quad \|v\|_{s_h}^2 = \|v\|_{s_h, F}^2 + \|v\|_{s_h, \Gamma}^2, \quad \|v\|_{A_h}^2 = \|v\|_{a_h}^2 + \|v\|_{s_h}^2. \quad (4.1)$$

We let $H^s(\omega)$, with $\omega \subset \mathbb{R}^d$, denote the standard Sobolev spaces of order s . For $\omega \subset \Gamma$ or $\omega \subset \Gamma_h$ $H^s(\omega)$ denotes the surface Sobolev space which is based on tangential derivatives.

4.2 Some Inequalities

- Under A1 and A2 there is a constant such that the following Poincaré inequality holds for $h \in (0, h_0]$,

$$\|v\|_{L^2(\Gamma_h)} \lesssim \|v\|_{a_h} \quad \forall v \in V_h^p, \quad (4.2)$$

see Lemma 4.1 in [3].

- For $T \in \mathcal{T}_h$ we have the trace inequalities

$$\|v\|_{L^2(\partial T)}^2 \lesssim h^{-1} \|v\|_{L^2(T)}^2 + h \|\nabla v\|_{L^2(T)}^2 \quad v \in H^1(T), \quad (4.3)$$

$$\|v\|_{L^2(T \cap \Gamma_h)}^2 \lesssim h^{-1} \|v\|_{L^2(T)}^2 + h \|\nabla v\|_{L^2(T)}^2 \quad v \in H^1(T), \quad (4.4)$$

where the first inequality is a standard trace inequality, see e.g. [1], and the second inequality is proven in [20] and the constant is independent of how Γ_h intersects T and of $h \in (0, h_0]$.

- For $T \in \mathcal{T}_h$ we have the inverse inequality

$$|v|_{H^j(T)}^2 \lesssim h^{-2(j-s)} \|v\|_{H^s(T)}^2 \quad 0 \leq s \leq j, \quad v \in V_h^p, \quad (4.5)$$

see [1].

4.3 Interpolation

Let $\pi_h^p : L^2(\mathcal{T}_h) \rightarrow V_h^p$ be the Clément interpolation operator. For all $v \in H^{p+1}(\mathcal{T}_h)$ and $T \in \mathcal{T}_h$ the following standard estimate holds

$$\|v - \pi_h^p v\|_{H^m(T)} \lesssim h^{s-m} \|v\|_{H^s(\mathcal{N}_h(T))} \quad m \leq s \leq p+1, \quad m = 0, \dots, p+1, \quad (4.6)$$

where $\mathcal{N}_h(T) \subset \mathcal{T}_h$ is the union of the elements in \mathcal{T}_h which share a node with T . In particular, we have the stability estimate

$$\|\pi_h^p v\|_{H^m(\mathcal{T}_h)} \lesssim \|v\|_{H^m(\mathcal{T}_h)}. \quad (4.7)$$

4.4 Some Results for Extended and Lifted Functions

Extension. Recall that we define the extension of a function u on Γ to $U_{\delta_0}(\Gamma)$ by $u^e(x) = u(p(x))$. For $u \in H^s(\Gamma)$, $s \geq 0$ the following holds

$$\|u^e\|_{H^s(U_{\delta_0}(\Gamma))} \lesssim \delta^{1/2} \|u\|_{H^s(\Gamma)}, \quad (4.8)$$

where $0 < \delta \leq \delta_0$ and for h small enough we may take $\delta \sim h$. See Lemma 3.1 in [29].

Using the definition of the extension of a function u on Γ , the definition of the closest point projection (2.2), the chain rule, and the identity $n = \nabla d$ we obtain

$$\nabla u^e = (P_\Gamma - dH)\nabla u \quad \text{in } U_{\delta_0}(\Gamma), \quad (4.9)$$

where $H(x) = D^2 d(x)$. For $x \in U_{\delta_0}(\Gamma)$, the eigenvalues of $H(x)$ are $\kappa_1(x)$, $\kappa_2(x)$, and 0, with corresponding orthonormal eigenvectors $a_1(x)$, $a_2(x)$, and $n^e(x)$. We have the identities

$$\kappa_i(x) = \frac{\kappa_i^e(x)}{1 + d(x)\kappa_i^e(x)}, \quad a_i(x) = a_i^e(x), \quad i = 1, 2 \quad (4.10)$$

and $H(x)$ may be expressed in the form

$$H(x) = \sum_{i=1}^2 \frac{\kappa_i^e(x)}{1 + d(x)\kappa_i^e(x)} a_i^e(x) \otimes a_i^e(x), \quad (4.11)$$

see [17, Lemma 14.7].

Using the fact that H is tangential, $P_\Gamma H = H P_\Gamma = H$, in the identity (4.9) we obtain

$$\nabla u^e = (I - dH)\nabla_\Gamma u. \quad (4.12)$$

Thus,

$$\nabla_{\Gamma_h} u^e = B^T \nabla_\Gamma u \quad (4.13)$$

with

$$B = P_\Gamma(I - dH)P_{\Gamma_h}. \quad (4.14)$$

Lifting. Define the lifting v^l of a function v on Γ_h to Γ as

$$(v^l)^e = v^l \circ p = v \quad \text{on } \Gamma_h. \quad (4.15)$$

Using equation (4.13) it follows that

$$\nabla_{\Gamma_h} v = \nabla_{\Gamma_h} (v^l)^e = B^T \nabla_{\Gamma} (v^l) \quad (4.16)$$

and thus we have

$$\nabla_{\Gamma} (v^l) = B^{-T} \nabla_{\Gamma_h} v. \quad (4.17)$$

Here,

$$B^{-1} = \left(I - \frac{n \otimes n_h}{n \cdot n_h} \right) (I - dH)^{-1}, \quad (4.18)$$

see [14], and using the fact that n and n_h are unit normals it is easy to show that

$$BB^{-1} = P_{\Gamma}, \quad B^{-1}B = P_{\Gamma_h}. \quad (4.19)$$

Estimates Related to B . It can be shown, see [3] for instance, that the following estimates hold

$$\|B\|_{L^\infty(\Gamma_h)} \lesssim 1, \quad \|B^{-1}\|_{L^\infty(\Gamma)} \lesssim 1, \quad \|BB^T - I\|_{L^\infty(\Gamma_h)} \lesssim h^{p+1}. \quad (4.20)$$

Surface Measures. For the surface measure on Γ_h , $ds_h(x)$, and the surface measure on Γ , $ds(p(x))$, we have the following identity

$$ds(p(x)) = |B(x)| ds_h(x), \quad x \in \Gamma_h, \quad (4.21)$$

where

$$|B(x)| = n \cdot n_h (1 - d(x)\kappa_1(x))(1 - d(x)\kappa_2(x)), \quad (4.22)$$

see Proposition A.1 in [14]. Using the identity $\|n(x) - n_h(x)\|_{\mathbb{R}^3}^2 = 2(1 - n(x) \cdot n_h(x))$ and our assumptions we obtain the following estimates:

$$\|1 - |B|\|_{L^\infty(\Gamma_h)} \lesssim h^{p+1}, \quad \| |B| \|_{L^\infty(\Gamma_h)} \lesssim 1, \quad \| |B|^{-1} \|_{L^\infty(\Gamma_h)} \lesssim 1. \quad (4.23)$$

Norm Equivalences. Using the identities (4.13) and (4.17) and the bounds in equations (4.20) and (4.23) we obtain the following equivalences

$$\|v^l\|_{L^2(\Gamma)} \sim \|v\|_{L^2(\Gamma_h)}, \quad \|u\|_{L^2(\Gamma)} \sim \|u^e\|_{L^2(\Gamma_h)}, \quad (4.24)$$

and

$$\|\nabla_{\Gamma} v^l\|_{L^2(\Gamma)} \sim \|\nabla_{\Gamma_h} v\|_{L^2(\Gamma_h)}, \quad \|\nabla_{\Gamma} u\|_{L^2(\Gamma)} \sim \|\nabla_{\Gamma_h} u^e\|_{L^2(\Gamma_h)}. \quad (4.25)$$

We will also use the following bound

$$\|D^j u^e\|_{L^2(\Gamma_h)} \lesssim \|u\|_{H^m(\Gamma)} \quad u \in H^m(\Gamma), \quad j \leq m. \quad (4.26)$$

The constant in (4.26) depends on the higher-order derivatives of the geometry.

5 Properties of the Stabilization Term

Here we formulate properties of a general stabilization term that are sufficient to prove that the resulting linear system of equations have an optimal scaling of the condition number with the mesh parameter and that the convergence of the method is of optimal order.

Properties. Let s_h be a semi positive definite bilinear form such that

P1. For $v \in H^{p+1}(\Gamma) \cap H_0^1(\Gamma)$,

$$\|v^e - \pi_h^p v^e\|_{s_h} \lesssim h^p \|v\|_{H^{p+1}(\Gamma)}. \quad (5.1)$$

P2. For $v \in H^{p+1}(\Gamma) \cap H_0^1(\Gamma)$,

$$\|v^e\|_{s_h} \lesssim h^p \|v\|_{H^{p+1}(\Gamma)}. \quad (5.2)$$

P3. For $v \in H^2(\Gamma)$,

$$\|\pi_h^p v^e\|_{s_h} \lesssim h \|v\|_{H^2(\Gamma)}. \quad (5.3)$$

P4. For $v \in V_h^p$,

$$\|v\|_{s_h}^2 \lesssim h^{-3} \|v\|_{L^2(\mathcal{T}_h)}^2. \quad (5.4)$$

P5. For $v \in V_h^p$,

$$\|v\|_{L^2(\mathcal{T}_h)}^2 \lesssim h(\|v\|_{a_h}^2 + \|v\|_{s_h}^2). \quad (5.5)$$

Remark 5.1 *The first three properties are used to establish the a priori error estimates: P1 is needed to show optimal interpolation error estimates, P2 is used to estimate the consistency error, and P3 is used to show optimal L^2 -error estimates. In P3 the assumption that $v \in H^2(\Gamma)$ reflects the fact that the solution to the dual problem resides in $H^2(\Gamma)$. The two last properties are used to show the condition number estimate: P4 is the inverse inequality and P5 is the Poincaré inequality. For the extension of these properties to the more general case of an n -dimensional smooth manifold embedded in \mathbb{R}^d , with codimension $cd = d - n$ see Section 7.*

Verification of P1–P5. We now show that the stabilization term defined in (3.7) satisfies P1-P5.

P1. Using a standard trace inequality on the faces (equation (4.3)) and the trace inequality

(4.4) for the contributions on Γ_h we obtain

$$\|w\|_{s_h}^2 = \sum_{j=1}^p \sum_{F \in \mathcal{F}_h} c_{F,j} h^{2(j-1+\gamma)} \| [D_{n_F}^j w] \|_{L^2(F)}^2 \quad (5.6)$$

$$\begin{aligned} &+ \sum_{j=1}^p \sum_{K \in \mathcal{K}_h} c_{\Gamma,j} h^{2(j-1+\gamma)} \| D_{n_h}^j w \|_{L^2(K)}^2 \\ &\lesssim \sum_{j=1}^p \sum_{T \in \mathcal{T}_h} h^{2(j-1+\gamma)} \left(h^{-1} \| D^j w \|_{L^2(T)}^2 + h \| D^{j+1} w \|_{L^2(T)}^2 \right) \end{aligned} \quad (5.7)$$

$$\lesssim \sum_{j=0}^p \sum_{T \in \mathcal{T}_h} h^{2(j+\gamma)-1} \| D^{j+1} w \|_{L^2(T)}^2 \quad (5.8)$$

$$= \sum_{j=0}^p h^{2(j+\gamma)-1} \| D^{j+1} w \|_{L^2(\mathcal{T}_h)}^2. \quad (5.9)$$

Next, setting $w = v^e - \pi_h^p v^e$, using the interpolation error estimate (4.6) and the stability (4.8) of the extension operator with $\delta \sim h$, we obtain

$$\|v^e - \pi_h^p v^e\|_{s_h}^2 \lesssim \sum_{j=0}^p h^{2(j+\gamma)-1} \| D^{j+1} (v^e - \pi_h^p v^e) \|_{L^2(\mathcal{T}_h)}^2 \quad (5.10)$$

$$\lesssim \sum_{j=0}^p h^{2(j+\gamma)-1} h^{2(p-j)} \| D^{j+1} v^e \|_{H^{p+1}(\mathcal{T}_h)}^2 \quad (5.11)$$

$$\lesssim h^{2(p+\gamma)} \|v\|_{H^{p+1}(\Gamma)}^2. \quad (5.12)$$

Finally, $h^{2(p+\gamma)} \lesssim h^{2p}$ for $\gamma \in [0, 1]$ since $h \in (0, h_0]$, and thus P1 follows.

P2. Note first that for $v \in H^{p+1}(\Gamma)$ we have $\|v^e\|_{s_{h,F}} = 0$ and thus $\|v^e\|_{s_h} = \|v^e\|_{s_{h,\Gamma}}$. Next, subtracting $D_n^j v^e = 0$, using Assumption A1, and inequality (4.26) we obtain

$$\|v^e\|_{s_h}^2 = \sum_{j=1}^p c_{\Gamma,j} h^{2(j-1+\gamma)} \| D_{n_h}^j v^e \|_{\mathcal{K}_h}^2 \quad (5.13)$$

$$\lesssim \sum_{j=1}^p h^{2(j-1+\gamma)} \| (D_{n_h}^j - D_n^j) v^e \|_{L^2(\mathcal{K}_h)}^2 \quad (5.14)$$

$$\lesssim \sum_{j=1}^p h^{2(j-1+\gamma)} \| n_h - n \|_{L^\infty(\mathcal{K}_h)}^2 \| D^j v^e \|_{L^2(\mathcal{K}_h)}^2 \quad (5.15)$$

$$\lesssim h^{2(p+\gamma)} \|v\|_{H^p(\Gamma)}^2, \quad (5.16)$$

where we used the estimate $\|n_h - n\|_{L^\infty(\mathcal{K}_h)} \lesssim h^p$. We conclude that P2 holds for $\gamma \in [0, 1]$ since $h \in (0, h_0]$.

P3. For $w \in V_h^p$ we have the estimate

$$\|w\|_{s_h}^2 \lesssim h^{2\gamma} \| [D_{n_F}^1 w] \|_{L^2(\mathcal{F}_h)}^2 + h^{2\gamma} \| D_{n_h}^1 w \|_{L^2(\mathcal{K}_h)}^2 + h^{2(1+\gamma)-1} \| D^2 w \|_{L^2(\mathcal{T}_h)}^2. \quad (5.17)$$

Verification of (5.17). We start from the definition

$$\|w\|_{s_h}^2 = \|w\|_{s_h,F}^2 + \|w\|_{s_h,\Gamma}^2 \quad (5.18)$$

and estimate the two terms on the right hand side as follows. First

$$\|w\|_{s_h,F}^2 \lesssim h^{2\gamma} \|[D_{n_F}^1 w]\|_{L^2(\mathcal{F}_h)}^2 + \sum_{j=2}^p h^{2(j-1+\gamma)} \|[D_{n_F}^j w]\|_{L^2(\mathcal{F}_h)}^2 \quad (5.19)$$

$$\lesssim h^{2\gamma} \|[D_{n_F}^1 w]\|_{L^2(\mathcal{F}_h)}^2 + h^{2(1+\gamma)-1} \|[D^2 w]\|_{L^2(\mathcal{T}_h)}^2, \quad (5.20)$$

where for each $j = 2, \dots, p$ and each face $F \in \mathcal{F}_h$ with neighboring elements T_1 and T_2 we used the inverse estimate

$$\|[D_{n_F}^j w]\|_{L^2(F)}^2 \lesssim h^{-1} \|D^j w\|_{L^2(T_1 \cup T_2)}^2 \lesssim h^{-1} h^{2(2-j)} \|D^2 w\|_{L^2(T_1 \cup T_2)}^2. \quad (5.21)$$

Second, using a similar approach

$$\|w\|_{s_h,\Gamma}^2 \lesssim h^{2\gamma} \|D_{n_h}^1 w\|_{L^2(\mathcal{K}_h)}^2 + \sum_{j=2}^p h^{2(j-1+\gamma)} \|D_{n_h}^j w\|_{L^2(\mathcal{K}_h)}^2 \quad (5.22)$$

$$\lesssim h^{2\gamma} \|D_{n_h}^1 w\|_{L^2(\mathcal{K}_h)}^2 + \sum_{j=2}^p \underbrace{h^{2(j-1+\gamma)} h^{-1} h^{2(2-j)}}_{=h^{2(1+\gamma)-1}} \|D^2 w\|_{L^2(\mathcal{T}_h)}^2 \quad (5.23)$$

$$\lesssim h^{2\gamma} \|D_{n_h}^1 w\|_{L^2(\mathcal{K}_h)}^2 + h^{2(1+\gamma)-1} \|D^2 w\|_{L^2(\mathcal{T}_h)}^2, \quad (5.24)$$

where we used the inverse estimate

$$\|D_{n_h}^j w\|_{L^2(K)}^2 \leq \|D^j w\|_{L^2(K)}^2 \lesssim h^{-1} \|D^j w\|_{L^2(T)}^2 \lesssim h^{-1} h^{2(2-j)} \|D^2 w\|_{L^2(T)}^2 \quad (5.25)$$

for $j = 2, \dots, p$. Thus (5.17) holds.

Setting $w = \pi_h^p v^e$ in (5.17) we obtain

$$\|\pi_h^p v^e\|_{s_h}^2 \lesssim \underbrace{h^{2\gamma} \|[D_{n_F}^1 \pi_h^p v^e]\|_{L^2(\mathcal{F}_h)}^2}_I + \underbrace{h^{2\gamma} \|D_{n_h}^1 \pi_h^p v^e\|_{L^2(\mathcal{K}_h)}^2}_{II} \quad (5.26)$$

$$+ h^{2(1+\gamma)-1} \|D^2 \pi_h^p v^e\|_{L^2(\mathcal{T}_h)}^2 \\ = I + II + h^{2(1+\gamma)} \|v\|_{H^2(\Gamma)}^2, \quad (5.27)$$

where we used the stability of the interpolation operator (4.7) and the stability of the extension operator (4.8). Next we have the following bounds.

Term I. Using the fact that $[D_{n_F}^1 v^e] = 0$ for $v \in H^2(\Gamma)$ we obtain

$$\|[D_{n_F}^1 \pi_h^p v^e]\|_{L^2(\mathcal{F}_h)}^2 = \|[D_{n_F}^1 (\pi_h^p v^e - v^e)]\|_{L^2(\mathcal{F}_h)}^2 \quad (5.28)$$

$$\lesssim h^{-1} \|[D(\pi_h^p v^e - v^e)]\|_{L^2(\mathcal{T}_h)}^2 + h \|[D^2(\pi_h^p v^e - v^e)]\|_{L^2(\mathcal{T}_h)}^2 \quad (5.29)$$

$$\lesssim h \|D^2 v^e\|_{L^2(\mathcal{T}_h)}^2 \quad (5.30)$$

$$\lesssim h^2 \|v\|_{H^2(\Gamma)}^2, \quad (5.31)$$

where we used the trace inequality (4.3), the interpolation estimate (4.6), and finally the stability (4.8) of the extension operator. Thus we have

$$I \lesssim h^{2(1+\gamma)} \|v\|_{H^2(\Gamma)}^2. \quad (5.32)$$

Term II. Using the fact that $D_{n^e}^1 v^e = 0$ we obtain

$$\|D_{n_h}^1 \pi_h^p v^e\|_{L^2(\mathcal{K}_h)}^2 \lesssim \|D_{n^e}^1 \pi_h^p v^e\|_{L^2(\mathcal{K}_h)}^2 + \|n^e - n_h\|_{L^\infty(\mathcal{K}_h)} \|D \pi_h^p v^e\|_{L^2(\mathcal{K}_h)}^2 \quad (5.33)$$

$$\lesssim \|D_{n^e}^1 (\pi_h^p v^e - v^e)\|_{L^2(\mathcal{K}_h)}^2 + h^{2p} \|D \pi_h^p v^e\|_{L^2(\mathcal{T}_h)}^2 \quad (5.34)$$

$$\lesssim h^2 \|v\|_{H^2(\Gamma)}^2 + h^{2p} \|v\|_{H^1(\Gamma)}^2 \quad (5.35)$$

and we arrive at

$$II \lesssim h^{2(1+\gamma)} \|v\|_{H^2(\Gamma)}^2 \quad (5.36)$$

since $p \geq 1$ and $h \in (0, h_0]$.

Collecting the bounds we obtain

$$\|\pi_h^p v^e\|_{s_h} \lesssim h^{1+\gamma} \|v\|_{H^2(\Gamma)} \quad (5.37)$$

and thus P3 holds.

Simplified Proof of P3 in the Case $\gamma = 1$. Using estimate (5.9) with $w \in V_h^p$ and inverse inequality (4.5) we obtain

$$\|w\|_{s_h}^2 \lesssim \sum_{j=0}^p h^{2j+1} \|D^{j+1} w\|_{L^2(\mathcal{T}_h)}^2 \quad (5.38)$$

$$\lesssim h \|Dw\|_{L^2(\mathcal{T}_h)}^2 + \underbrace{\sum_{j=1}^p h^{2j+1} \|D^{j+1} w\|_{L^2(\mathcal{T}_h)}^2}_{\lesssim h^3 \|D^2 w\|_{L^2(\mathcal{T}_h)}^2} \quad (5.39)$$

$$\lesssim h \|Dw\|_{L^2(\mathcal{T}_h)}^2 + h^3 \|D^2 w\|_{L^2(\mathcal{T}_h)}^2. \quad (5.40)$$

Setting $w = \pi_h^p v^e$ and using the stability of the interpolation operator (4.7) and the stability of the extension operator (4.8) we obtain

$$\|\pi_h^p v^e\|_{s_h}^2 \lesssim h \|D \pi_h^p v^e\|_{L^2(\mathcal{T}_h)}^2 + h^3 \|D^2 \pi_h^p v^e\|_{L^2(\mathcal{T}_h)}^2 \quad (5.41)$$

$$\lesssim h^2 \|v\|_{H^1(\Gamma)}^2 + h^4 \|v\|_{H^2(\Gamma)}^2. \quad (5.42)$$

P4. Starting from (5.9) with $w \in V_h^p$ and using the inverse inequality we get

$$\|w\|_{s_h}^2 \lesssim \sum_{j=0}^p h^{2j+2\gamma-1} \|D^{j+1} w\|_{L^2(\mathcal{T}_h)}^2 \lesssim h^{2\gamma-3} \|w\|_{L^2(\mathcal{T}_h)}^2. \quad (5.43)$$

Using that $h \in (0, h_0]$ we have $h^{2\gamma-3} \lesssim h^{-3}$ for $\gamma \geq 0$ and thus Property P4 holds.

P5. See the proof of Lemma 6.3 below.

Remark 5.2 We note that the normal gradient stabilization (1.10) satisfies P_1, P_2, P_4 , and P_5 , see [18] and [5]. To verify P_3 we use that $n^e \cdot \nabla v^e = 0$, interpolation error estimates,

the H^1 -stability of the interpolant, assumption A2 (the inclusion $\mathcal{T}_h \subset U_\delta(\Gamma)$ with $\delta \sim h$), the stability of the extension operator (4.8), and that $\|n_h - n^e\|_{L^\infty(\mathcal{T}_h)}^2 \lesssim h^{2p}$ to conclude that

$$\|\pi_h^p v^e\|_{s_h}^2 \lesssim h^\alpha \left(\|n^e \cdot \nabla \pi_h^p v^e\|_{L^2(\mathcal{T}_h)}^2 + \|n_h - n^e\|_{L^\infty(\mathcal{T}_h)}^2 \|\nabla \pi_h^p v^e\|_{L^2(\mathcal{T}_h)}^2 \right) \quad (5.44)$$

$$\lesssim h^\alpha \left(\|n^e \cdot \nabla (\pi_h^p v^e - v^e)\|_{L^2(\mathcal{T}_h)}^2 + h^{2p} \delta \|v\|_{H^1(\Gamma)}^2 \right) \lesssim h^\alpha h^2 \delta \|v\|_{H^2(\Gamma)}^2 \quad (5.45)$$

$$\lesssim h^{3+\alpha} \|v\|_{H^2(\Gamma)}^2. \quad (5.46)$$

We also used that $p \geq 1$. Thus we conclude that P_3 holds for $\alpha \geq -1$.

6 Condition Number Estimate

We shall show that the spectral condition number of the resulting stiffness matrix scales as h^{-2} , independent of the position of the geometry relative to the background mesh. In particular, we show that the stabilization term defined in (3.7) has Property P5 and controls the condition number for linear as well as for higher-order elements.

Let $\{\varphi_i\}_{i=1}^N$ be a basis in V_h^p and given $v \in V_h^p$ let $\hat{v} \in \hat{\mathbb{R}}^N \subset \mathbb{R}^N$ denote the vector containing the coefficients in the expansion:

$$v = \sum_{i=1}^N \hat{v}_i \varphi_i. \quad (6.1)$$

Recall that functions v in V_h^p satisfy the condition $\int_{\Gamma_h} v ds_h = 0$ and therefore $\hat{\mathbb{R}}^N$ is

$$\hat{\mathbb{R}}^N = \{\hat{v} \in \mathbb{R}^N \mid \hat{v} \cdot \left(\int_{\Gamma_h} \varphi_1 ds_h, \dots, \int_{\Gamma_h} \varphi_N ds_h \right) = 0\}. \quad (6.2)$$

Since \mathcal{T}_h is quasi-uniform we have the equivalence

$$\|v\|_{\mathcal{T}_h} \sim h^{d/2} \|\hat{v}\|_{\hat{\mathbb{R}}^N}, \quad (6.3)$$

where d is the dimension of the embedding space \mathbb{R}^d . Let \mathcal{A}_h be the stiffness matrix associated with A_h ,

$$(\mathcal{A}_h \hat{w}, \hat{v})_{\hat{\mathbb{R}}^N} = A_h(w, v) \quad \forall v, w \in V_h^p \quad (6.4)$$

and recall that the condition number is defined by

$$\kappa(\mathcal{A}_h) = \|\mathcal{A}_h\|_{\mathbb{R}^N} \|\mathcal{A}_h^{-1}\|_{\mathbb{R}^N} \quad (6.5)$$

which in terms of the eigenvalues of the symmetric positive definite matrix \mathcal{A}_h is equal to

$$\kappa(\mathcal{A}_h) = \frac{\lambda_N}{\lambda_1}, \quad (6.6)$$

where λ_N (λ_1) is the largest (smallest) eigenvalue of \mathcal{A}_h .

Theorem 6.1 *If there are constants, independent of the mesh size h and of how the surface cuts the background mesh, such that the following hold:*

- A_h is continuous: $A_h(w, v) \lesssim \|w\|_{A_h} \|v\|_{A_h} \quad \forall v, w \in V_h^p + H^{p+1}(\mathcal{T}_h)$
- A_h is coercive: $\|v\|_{A_h}^2 \lesssim A_h(v, v) \quad \forall v \in V_h^p$
- The inverse inequality: $\|v\|_{A_h} \lesssim h^{-3/2} \|v\|_{L^2(\mathcal{T}_h)} \quad v \in V_h^p$
- The Poincaré inequality: $\|v\|_{L^2(\mathcal{T}_h)} \lesssim h^{1/2} \|v\|_{A_h} \quad v \in V_h^p$

Then, the spectral condition number $\kappa(\mathcal{A}_h)$ satisfies

$$\kappa(\mathcal{A}_h) \lesssim h^{-2}. \quad (6.7)$$

Proof. For $v, w \in V_h^p$ it follows from the continuity of the form A_h , the inverse inequality, and the equivalence between the norms, equation (6.3), that

$$A_h(w, v) \lesssim \|w\|_{A_h} \|v\|_{A_h} \lesssim h^{-3} \|w\|_{L^2(\mathcal{T}_h)} \|v\|_{L^2(\mathcal{T}_h)} \lesssim h^{-3} h^d \|\widehat{w}\|_{\widehat{\mathbb{R}}^N} \|\widehat{v}\|_{\widehat{\mathbb{R}}^N}. \quad (6.8)$$

From coercivity, the Poincaré inequality, and the equivalence between the norms, equation (6.3), we obtain

$$A_h(v, v) \gtrsim \|v\|_{A_h}^2 \gtrsim h^{-1} \|v\|_{L^2(\mathcal{T}_h)}^2 \gtrsim h^{-1} h^d \|\widehat{v}\|_{\widehat{\mathbb{R}}^N}^2. \quad (6.9)$$

Using the definition (6.6) of the spectral condition number we get

$$\kappa(\mathcal{A}_h) = \frac{\max_{u \in \widehat{\mathbb{R}}^N, \|\widehat{u}\|_{\widehat{\mathbb{R}}^N} = 1} (\mathcal{A}_h \widehat{u}, \widehat{u})_{\widehat{\mathbb{R}}^N}}{\min_{u \in \widehat{\mathbb{R}}^N, \|\widehat{u}\|_{\widehat{\mathbb{R}}^N} = 1} (\mathcal{A}_h \widehat{u}, \widehat{u})_{\widehat{\mathbb{R}}^N}} \lesssim \frac{h^{-3} h^d}{h^{-1} h^d} = h^{-2}. \quad (6.10)$$

□

In the following Lemmas we show that all the conditions in Theorem 6.1 are satisfied.

Lemma 6.1 (*Continuity and Inf-Sup Condition*) *There is a constant independent of the mesh size h and of how the surface cuts the background mesh, such that A_h is continuous:*

$$A_h(w, v) \leq \|w\|_{A_h} \|v\|_{A_h}, \quad \forall v, w \in V_h^p + H^{p+1}(\mathcal{T}_h) \quad (6.11)$$

and A_h satisfies the inf-sup condition

$$\|w\|_{A_h} \lesssim \sup_{v \in V_h^p \setminus \{0\}} \frac{A_h(w, v)}{\|v\|_{A_h}}, \quad \forall w \in V_h^p. \quad (6.12)$$

Proof. The continuity follows directly from the Cauchy-Schwarz inequality. The bilinear form A_h is coercive $A_h(v, v) = \|v\|_{A_h}^2$ by definition and the inf-sup condition (6.12) follows from coercivity. □

Lemma 6.2 (*Inverse Inequality*) *There are constants, independent of the mesh size h and of how the surface cuts the background mesh, such that the following inverse inequality holds*

$$\|v\|_{A_h} \lesssim h^{-3/2} \|v\|_{L^2(\mathcal{T}_h)} \quad v \in V_h^p. \quad (6.13)$$

Proof. Using the element wise trace inequality (4.4), the inverse inequality (4.5), and Property P4 of the stabilization term we obtain

$$\begin{aligned} \|v\|_{a_h}^2 &\lesssim h^{-1} \|v\|_{H^1(\mathcal{T}_h)}^2 + h \|v\|_{H^2(\mathcal{T}_h)}^2 \lesssim h^{-3} \|v\|_{L^2(\mathcal{T}_h)}^2, \\ \|v\|_{s_h}^2 &\lesssim h^{-3} \|v\|_{L^2(\mathcal{T}_h)}^2. \end{aligned} \quad (6.14)$$

Using the above estimates and recalling the definition of $\|v\|_{A_h}$ the result follows. \square

Lemma 6.3 (*Poincaré Inequality*) *There are constants, independent of the mesh size h and of how the surface cuts the background mesh, such that the following Poincaré inequality holds*

$$\|v\|_{L^2(\mathcal{T}_h)} \lesssim h^{1/2} \|v\|_{A_h} \quad v \in V_h^p. \quad (6.15)$$

Proof. To prove the Poincaré inequality we will proceed in two main steps: 1. We use the face penalty to reach an element which has a large intersection with Γ_h . Here we employ a covering of \mathcal{T}_h , where each covering set contains elements that have a so called large intersection property, see [3]. 2. For elements with a large intersection the normal derivative control on Γ_h is used to control the L^2 norm on the element.

To establish the Poincaré inequality (6.15) we shall prove that

$$\|v\|_{L^2(\mathcal{T}_h)}^2 \lesssim \sum_{j=0}^p h^{2j+1} \|D_{n_h}^j v\|_{L^2(\Gamma_h)}^2 + \sum_{j=1}^p h^{2j+1} \|[D_{n_F}^j v]\|_{L^2(\mathcal{F}_h)}^2. \quad (6.16)$$

Here we note that (6.15) follows from (6.16) since the right hand side of (6.16) satisfies the estimate

$$\begin{aligned} &\sum_{j=0}^p h^{2j+1} \|D_{n_h}^j v\|_{L^2(\Gamma_h)}^2 + \sum_{j=1}^p h^{2j+1} \|[D_{n_F}^j v]\|_{L^2(\mathcal{F}_h)}^2 \\ &\lesssim h(\|v\|_{\Gamma_h}^2 + h^{2(1-\gamma)} \|v\|_{s_h}^2) \lesssim h(\|v\|_{a_h}^2 + h^{2(1-\gamma)} \|v\|_{s_h}^2) \lesssim h \|v\|_{A_h}^2, \end{aligned} \quad (6.17)$$

where we used the definition (3.7) of s_h , the Poincaré inequality (4.2), and the fact that $\gamma \in [0, 1]$.

Large Intersection Coverings of \mathcal{T}_h . There is a covering $\{\mathcal{T}_{h,x} : x \in \mathcal{X}_h\}$ of \mathcal{T}_h , where \mathcal{X}_h is an index set, such that: (1) Each set $\mathcal{T}_{h,x}$ contains a uniformly bounded number of elements. (2) Each element in $\mathcal{T}_{h,x}$ share at least one face with another element in $\mathcal{T}_{h,x}$. (3) In each set $\mathcal{T}_{h,x}$ there is one element $T_x \in \mathcal{T}_{h,x}$ which has a large intersection with Γ_h ,

$$h^{d-1} \lesssim |T_x \cap \Gamma_h| = |K_x|, \quad (6.18)$$

where d is the dimension. (4) The number of sets $\mathcal{T}_{h,x}$ to which an element T belongs is uniformly bounded for all $T \in \mathcal{T}_h$. See [3] for the construction of the covering.

We prove (6.16) by considering a set $\mathcal{T}_{h,x}$ in the covering and the following steps:

Step 1. We shall show that

$$\|v\|_{L^2(\mathcal{T}_{h,x})}^2 \lesssim \|v\|_{L^2(T_x)}^2 + \sum_{j=1}^p h^{2j+1} ([D_{n_F}^j v], [D_{n_F}^j w])_{\mathcal{F}_{h,x}}, \quad (6.19)$$

where $\mathcal{F}_{h,x}$ is the set of interior faces in $\mathcal{T}_{h,x}$. To prove (6.19) we recall that for two elements T_1 and T_2 that share a face F it holds

$$\|v\|_{L^2(T_1)}^2 \lesssim \|v\|_{L^2(T_2)}^2 + \sum_{j=1}^p h^{2j+1} \| [D_{n_F}^j v] \|_{L^2(F)}^2, \quad (6.20)$$

see [21] for instance. Now let $\mathcal{T}_{h,x}^0 = \{T_x\}$ and for $j = 1, 2, \dots$ let $\mathcal{T}_{h,x}^j$ be the set of all elements that share a face with an element in $\mathcal{T}_{h,x}^{j-1}$. Then there is a uniform constant J such that $\mathcal{T}_{h,x}^j = \mathcal{T}_{h,x}^{j-1}$ for $j \geq J$ and we also have the estimate

$$\|v\|_{\mathcal{T}_{h,x}^j} \lesssim \|v\|_{\mathcal{T}_{h,x}^{j-1}} + \sum_{F \subset \mathcal{F}_{h,x}^j \setminus \mathcal{F}_{h,x}^{j-1}} \sum_{j=1}^p h^{2j+1} \| [D_{n_F}^j v] \|_{L^2(F)}^2, \quad (6.21)$$

where $\mathcal{F}_{h,x}^j$ is the set of interior faces in $\mathcal{T}_{h,x}^j$. Iterating (6.21) we obtain (6.19).

Step 2. We shall show that there is a constant such that for all $T_x \in \mathcal{T}_h$ which have the large intersection property (6.18),

$$\|v\|_{L^2(T_x)}^2 \lesssim \sum_{j=0}^p h^{2j+1} \| D_{n_h}^j v \|_{L^2(K_x)}^2 \quad (6.22)$$

where $K_x = \Gamma_h \cap T_x$. To verify (6.22) we define the cylinder

$$\text{Cyl}_\delta(K_x) = \{x \in \mathbb{R}^d : x = y + tn_h, y \in K_x, |t| \leq \delta\} \quad (6.23)$$

and using Taylor's formula for a polynomial $v \in P_p(\text{Cyl}_\delta(K_x))$, we obtain the bound

$$\|v\|_{L^2(\text{Cyl}_\delta(K_x))}^2 \lesssim \sum_{j=0}^p \delta^{2j+1} \| D_{n_h}^j v \|_{L^2(K_x)}^2. \quad (6.24)$$

Using the following estimate, which we verify below, there is a constant such that for all $v \in P_p(T_x)$,

$$\|v\|_{L^2(T_x)} \lesssim \|v\|_{L^2(\text{Cyl}_\delta(K_x))}, \quad (6.25)$$

the desired estimate (6.22) follows for $\delta \sim h$.

Verification of (6.25). To employ a scaling argument we will construct two regular cylinders with circular cross section and the same center line that may be mapped to a reference configuration, one containing T_x and one contained in $\text{Cyl}_\delta(K_x)$. See Figure 6.

Let \bar{F}_x be a plane with unit normal \bar{n}_x , which is tangent to K_x at an interior point of K_x . Then we have the bound

$$\|\bar{n}_h - n_h\|_{L^\infty(K_x)} \lesssim h \quad (6.26)$$

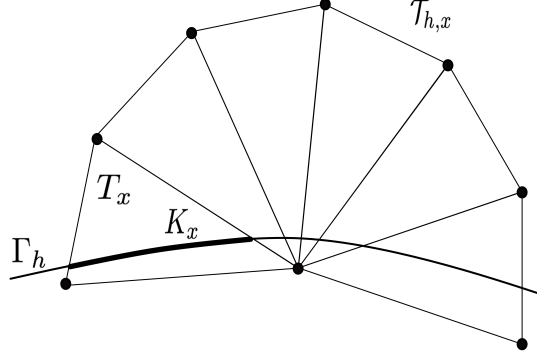


Figure 2: A set of elements $\mathcal{T}_{h,x}$ in the cover of \mathcal{T}_h , an element T_x with large intersection $K_x = T_x \cap \Gamma_h$.

and with \bar{K}_x the closest point projection of K_x onto \bar{F}_x we conclude using shape regularity and a uniform bound on the curvature κ_h (Assumption A1) that there is a ball $\bar{B}_{\bar{r}_1,x} \subset \bar{K}_x \subset \bar{F}_x$ with radius $\bar{r}_1 \sim h$ and a $\bar{\delta}_1 \sim h$ such that

$$\text{Cyl}_{\bar{\delta}_1}(\bar{K}_x) = \{x \in \mathbb{R}^d : x = y + t\bar{n}_h, y \in \bar{K}_x, |t| \leq \bar{\delta}_1\} \subset \text{Cyl}_{\bar{\delta}}(K_x). \quad (6.27)$$

Next using shape regularity there is a larger ball $\bar{B}_{\bar{r}_2,x} \subset \bar{F}_x$ with the same center as $\bar{B}_{\bar{r}_1,x}$ such that

$$\bar{T}_x \subset \bar{B}_{\bar{r}_2,x} \subset \bar{F}_x, \quad (6.28)$$

where \bar{T}_x is the closest point projection of T_x onto \bar{F}_x , and a $\bar{\delta}_2 \sim h$ such that

$$T_x \subset \text{Cyl}_{\bar{\delta}_2}(\bar{B}_{\bar{r}_2,x}). \quad (6.29)$$

Clearly, $\text{Cyl}_{\bar{\delta}_1}(\bar{B}_{\bar{r}_1,x}) \subset \text{Cyl}_{\bar{\delta}_2}(\bar{B}_{\bar{r}_2,x})$ and using a mapping to a reference configuration we conclude that there is a constant such that for all polynomials $v \in P_p(\text{Cyl}_{\bar{\delta}_2}(\bar{B}_{\bar{r}_2,x}))$,

$$\|v\|_{\text{Cyl}_{\bar{\delta}_2}(\bar{B}_{\bar{r}_2,x})} \lesssim \|v\|_{\text{Cyl}_{\bar{\delta}_1}(\bar{B}_{\bar{r}_1,x})} \quad (6.30)$$

which in view of the inclusions (6.27) and (6.29) concludes the proof of (6.25).

Step 3. Combining equation (6.19) and (6.22) and using that $\{\mathcal{T}_{h,x} : x \in \mathcal{X}_h\}$ is a cover of \mathcal{T}_h completes the proof of (6.16) and the lemma. \square

Remark 6.1 Using the same technique as in the proof of Lemma 6.3 we may show the stronger estimate

$$\|v\|_{\mathcal{T}_h}^2 + h^{2\gamma} \|\nabla v\|_{\mathcal{T}_h}^2 \lesssim h \|v\|_{A_h}^2, \quad (6.31)$$

where $\gamma \in [0, 1]$ is the scaling parameter in s_h , see (3.8) and (3.9). The modifications are as follows. In Step 1 we show that

$$\|\nabla v\|_{L^2(\mathcal{T}_{h,x})}^2 \lesssim \|\nabla v\|_{L^2(T_x)}^2 + \sum_{j=1}^p h^{2j-1} \|[D_{n_F}^j v]\|_{L^2(F)}^2 \quad (6.32)$$

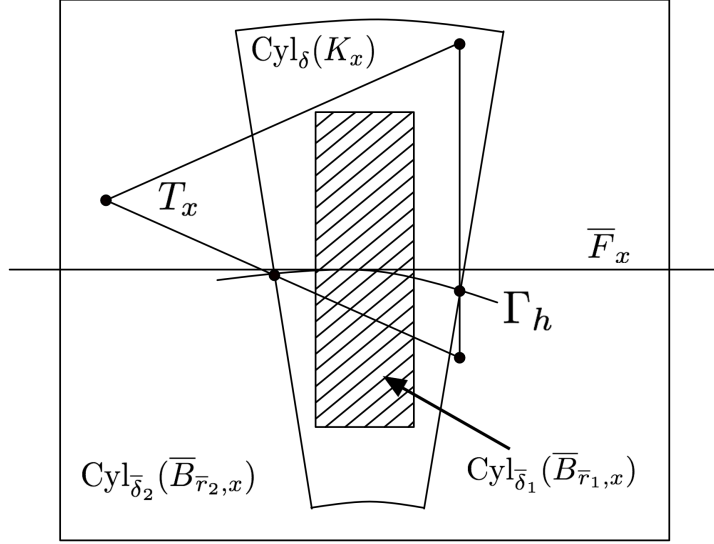


Figure 3: Schematic figure illustrating a typical configuration of an element T , the curved intersection with Γ_h , the plane \bar{F}_x which is tangent to K_x , the cylinders $\text{Cyl}_\delta(K_x)$, $\text{Cyl}_{\delta_1}(\bar{B}_{\bar{r}_1})$, and $\text{Cyl}_{\delta_2}(\bar{B}_{\bar{r}_2})$. Note that we have the inclusions $\bar{B}_{\bar{r}_1, x} \subset \bar{K}_x \subset \bar{T}_x \subset \bar{B}_{\bar{r}_2, x}$, $T_x \subset \text{Cyl}_{\delta_2}(\bar{B}_{\bar{r}_2})$, and $\text{Cyl}_{\delta_1}(\bar{B}_{\bar{r}_1}) \subset \text{Cyl}_\delta(K_x)$.

which after multiplication by $h^{2\gamma}$ corresponds to

$$h^{2\gamma} \|\nabla v\|_{L^2(\mathcal{T}_{h,x})}^2 \lesssim h^{2\gamma} \|\nabla v\|_{L^2(T_x)}^2 + h \left(\sum_{j=1}^p h^{2(j-1+\gamma)} \| [D_{n_F}^j v] \|_{L^2(F)}^2 \right). \quad (6.33)$$

To show (6.32) we use the estimate

$$\|\nabla v\|_{L^2(T_1)}^2 \lesssim \|\nabla v\|_{L^2(T_2)}^2 + \sum_{j=1}^p h^{2j-1} \| [D_{n_F}^j v] \|_{L^2(F)}^2. \quad (6.34)$$

In Step 2 we show that

$$\|\nabla v\|_{L^2(T_x)}^2 \lesssim \|\nabla_{\Gamma_h} v\|_{K_x}^2 + \sum_{j=1}^p h^{2j-1} \| D_{n_h}^j v \|_{L^2(K_x)}^2 \quad (6.35)$$

which after multiplication by $h^{2\gamma}$ corresponds to

$$h^{2\gamma} \|\nabla v\|_{L^2(T_x)}^2 \lesssim \underbrace{h^{2\gamma} \|\nabla_{\Gamma_h} v\|_{K_x}^2}_{\lesssim \|\nabla_{\Gamma_h} v\|_{K_x}^2} + h \left(\sum_{j=1}^p h^{2(j-1+\gamma)} \| D_{n_h}^j v \|_{L^2(K_x)}^2 \right). \quad (6.36)$$

Combining (6.33) and (6.36), summing over the cover, and using Property (4) of the cover we obtain (6.31).

Remark 6.1 Note the following:

- From (5.43) we see that the scaling of the stabilization term corresponds to the mass matrix. This scaling is the weakest which guarantees the Poincaré inequality (6.15) (Property P4 of the stabilization term).
- For the operator

$$L = \alpha\Delta_\Gamma + \beta \quad (6.37)$$

where α and β are constants, we would have the inverse inequality

$$\|v\|_{A_h} \lesssim (\alpha h^{-3/2} + \beta h^{-1/2}) \|v\|_{\mathcal{T}_h} \quad v \in V_h^p \quad (6.38)$$

instead of (6.13), and the resulting condition number estimate is then

$$\kappa(\mathcal{A}_h) \lesssim \alpha h^{-2} + \beta. \quad (6.39)$$

- In the case when

$$\|v\|_{a_h} \lesssim (\alpha h^{-3/2} + \beta h^{-1/2}) \|v\|_{\mathcal{T}_h} \quad (6.40)$$

we note that the desired inverse inequality (6.38) holds for

$$\tilde{s}_h = (\alpha h^{-\tau} + \beta) s_h, \quad (6.41)$$

with τ in the interval $0 \leq \tau \leq 2$, since

$$\|v\|_{\tilde{s}_h}^2 = (\alpha h^{-\tau} + \beta) \|v\|_{s_h}^2 \lesssim (\alpha h^{-\tau} + \beta) h^{-1} \|v\|_{\mathcal{T}_h}^2 \lesssim (\alpha h^{-(1+\tau)} + \beta h^{-1}) \|v\|_{\mathcal{T}_h}^2. \quad (6.42)$$

7 Extension to Problems on Manifolds with General Codimension Embeddings

The stabilization term (3.7) may be extended to the more general case of an n -dimensional smooth manifold embedded in \mathbb{R}^d , with codimension $cd = d - n > 1$, by scaling the face penalty term (3.8) in such a way that the stabilization terms associated with the faces and surface scale in the same way,

$$s_{h,F}(w, v) = \sum_{j=1}^p c_{F,j} h^{2(j-1+\gamma)} h^{1-cd} ([D_{n_F}^j w], [D_{n_F}^j v])_{\mathcal{F}_h}, \quad (7.1)$$

$$s_{h,\Gamma}(w, v) = \sum_{j=1}^p c_{\Gamma,j} h^{2(j-1+\gamma)} (D_{n_h}^j w, D_{n_h}^j v)_{\mathcal{K}_h}. \quad (7.2)$$

This is the same scaling as is used for the face stabilization term in the case of piecewise linear elements in general codimension, see Table 1 in [5]. With this definition P1-P3 remain the same and may be verified using the results in [5]. P4-P5 take the more general form

P4. For $v \in V_h^p$,

$$\|v\|_{s_h}^2 \lesssim h^{-(cd+2)} \|v\|_{L^2(\mathcal{T}_h)}^2. \quad (7.3)$$

P5. For $v \in V_h^p$,

$$\|v\|_{L^2(\mathcal{T}_h)}^2 \lesssim h^{cd} (\|v\|_{a_h}^2 + \|v\|_{s_h}^2). \quad (7.4)$$

P4 is verified as in equation (5.43) and below we comment on the minor modifications in the proof of Lemma 6.3 necessary to verify P5.

We next extend the proof of Lemma 6.3, to the case of a general embedding of an n -dimensional surface in \mathbb{R}^d . To that end we first note that Step 1 can be directly carried out for d -dimensional simplices and we obtain

$$\|v\|_{L^2(\mathcal{T}_{h,x})}^2 \lesssim \|v\|_{L^2(T_x)}^2 + h^{cd} \left(\sum_{j=1}^p h^{2j} h^{1-cd} ([D_{n_F}^j v], [D_{n_F}^j w])_{\mathcal{F}_{h,x}} \right). \quad (7.5)$$

For Step 2, the only difference is that we will have $cd = d - n$ orthonormal normal directions $\{n_{h,i}\}_{i=1}^{cd}$, which we may choose to vary smoothly over K_x , see [5] for details, and therefore the definition of the cylinder over K_x takes the form

$$\text{Cyl}_\delta(K_x) = \{x \in \mathbb{R}^d : x = y + \sum_{i=1}^{cd} t_i n_{h,i}, y \in K_x, |t_i| \leq \delta, i = 1, \dots, cd\}. \quad (7.6)$$

Using Taylor's formula in several dimensions and integrating over the cylinder (7.6), we obtain the following generalization of (6.24),

$$\|v\|_{L^2(\text{Cyl}_\delta(K_x))}^2 \lesssim \sum_{j=0}^p \delta^{2j+cd} \|D_{n_h}^j v\|_{L^2(K_x)}^2 \quad (7.7)$$

where we used the fact that, for a monomial $\prod_{i=1}^{cd} x_i^{2l_i}$, with $\sum_{i=1}^{cd} l_i = j$, it holds

$$\int_{[-\delta, \delta]^{cd}} \prod_{i=1}^{cd} x_i^{2l_i} = \prod_{i=1}^{cd} \int_{-\delta}^{\delta} x_i^{2l_i} dx_i \sim \prod_{i=1}^{cd} \delta^{2l_i+1} = \delta^{2j+cd}. \quad (7.8)$$

We finally note that (6.25) holds in any dimension d and the desired estimate in Step 2 follows for $\delta \sim h$, and Step 3 is just a combination of Step 1 and 2. Thus the proof of Lemma 6.3 easily extends to the case of general codimension embeddings and we conclude that (7.4) holds.

8 A Priori Error Estimates

In this section we prove optimal error estimates in the energy norm and in the L^2 norm.

8.1 Strang Lemma

Using that A_h is continuous and satisfies the inf-sup condition we first show a Strang Lemma which connects the error in the energy norm to the interpolation error and the consistency error.

Lemma 8.1 *Let $u \in H_0^1(\Gamma)$ be the unique solution of (2.5) and $u_h \in V_h^p$ the finite element approximation defined by (3.3). Then the following discretization error bound holds*

$$\|u^e - u_h\|_{A_h} \lesssim \|u^e - \pi_h^p u^e\|_{A_h} + \sup_{v \in V_h^p \setminus \{0\}} \frac{|A_h(u^e, v) - l_h(v)|}{\|v\|_{A_h}}. \quad (8.1)$$

Proof. Adding and subtracting an interpolant and using the triangle inequality we get

$$\|u^e - u_h\|_{A_h} \leq \|u^e - \pi_h^p u^e\|_{A_h} + \|\pi_h^p u^e - u_h\|_{A_h}. \quad (8.2)$$

Using the inf-sup condition (6.12) for A_h we have

$$\|\pi_h^p u^e - u_h\|_{A_h} \lesssim \sup_{v \in V_h^p \setminus \{0\}} \frac{A_h(\pi_h^p u^e - u_h, v)}{\|v\|_{A_h}}. \quad (8.3)$$

Adding and subtracting $A_h(u^e, v)$ and using the weak formulation (3.3) yields

$$A_h(\pi_h^p u^e - u_h, v) = A_h(\pi_h^p u^e - u^e, v) + A_h(u^e - u_h, v) \quad (8.4)$$

$$= A_h(\pi_h^p u^e - u^e, v) + A_h(u^e, v) - l_h(v). \quad (8.5)$$

Finally, using the continuity of A_h we obtain

$$A_h(\pi_h^p u^e - u^e, v) \leq \|\pi_h^p u^e - u^e\|_{A_h} \|v\|_{A_h}. \quad (8.6)$$

Collecting the estimates we end up with the desired bound

$$\|u^e - u_h\|_{A_h} \lesssim \|u^e - \pi_h^p u^e\|_{A_h} + \sup_{v \in V_h^p \setminus \{0\}} \frac{|A_h(u^e, v) - l_h(v)|}{\|v\|_{A_h}}. \quad (8.7)$$

□

8.2 The Interpolation Error

Next we prove optimal interpolation error estimates using Property P1 of the stabilization term.

Lemma 8.2 *For all $u \in H^{p+1}(\Gamma)$ we have the following estimate*

$$\|u^e - \pi_h^p u^e\|_{A_h} \lesssim h^p \|u\|_{H^{p+1}(\Gamma)}. \quad (8.8)$$

Proof. From the definition of the energy norm $\|\cdot\|_{A_h}$, equation (4.1), we have

$$\|u^e - \pi_h^p u^e\|_{A_h}^2 = \underbrace{\|u^e - \pi_h^p u^e\|_{a_h}^2}_I + \underbrace{\|u^e - \pi_h^p u^e\|_{s_h}^2}_{II}. \quad (8.9)$$

Term I. Using the element wise trace inequality (4.4), standard interpolation estimates (4.6) on elements $T \in \mathcal{T}_h$, and the stability estimate (4.8) for the extension operator with $\delta \sim h$, we obtain

$$I = \|u^e - \pi_h^p u^e\|_{a_h}^2 \quad (8.10)$$

$$\lesssim \sum_{T \in \mathcal{T}_h} \left(h^{-1} \|u^e - \pi_h^p u^e\|_{H^1(T)}^2 + h \|u^e - \pi_h^p u^e\|_{H^2(T)}^2 \right) \quad (8.11)$$

$$\lesssim h^{2p} \|u\|_{H^{p+1}(\Gamma)}^2. \quad (8.12)$$

Term II. From Property P1 of the stabilization term we have that

$$II \lesssim h^{2p} \|u\|_{H^{p+1}(\Gamma)}^2. \quad (8.13)$$

Combining the two estimates (8.10) and (8.13) the result follows. \square

8.3 The Consistency Error

The approximation of the geometry Γ by Γ_h and the approximation of the data f by f_h leads to a consistency error that we estimate in the next lemma.

Lemma 8.3 *Let $u \in H^{p+1}(\Gamma) \cap H_0^1(\Gamma)$ be the solution of (2.5) then, the following bound holds*

$$\sup_{v \in V_h^p \setminus \{0\}} \frac{|A_h(u^e, v) - l_h(v)|}{\|v\|_{A_h}} \lesssim h^p \|u\|_{H^{p+1}(\Gamma)} + h^{p+1} \|f\|_{L^2(\Gamma)}. \quad (8.14)$$

Proof. We have the identity

$$|A_h(u^e, v) - l_h(v)| \leq \underbrace{|a_h(u^e, v) - l_h(v)|}_I + \underbrace{|s_h(u^e, v)|}_{II}. \quad (8.15)$$

Term I. Adding $-a(u, v^l) + l(v^l) = 0$, and using the triangle inequality

$$I \leq \underbrace{|a_h(u^e, v) - a(u, v^l)|}_{I_I} + \underbrace{|l(v^l) - l_h(v)|}_{I_{II}}. \quad (8.16)$$

Term I_I . Adding and subtracting $\int_{\Gamma_h} \nabla_{\Gamma_h} u^e \cdot \nabla_{\Gamma_h} v |B| ds_h$, using that $B^T B^{-T} = P_{\Gamma_h}$, changing the domain of integration from Γ to Γ_h , using the triangle inequality, norm equivalences in (4.25), estimates (4.20), and (4.23) we obtain

$$\begin{aligned} |a_h(u^e, v) - a(u, v^l)| &= \left| \int_{\Gamma_h} (1 - |B|) \nabla_{\Gamma_h} u^e \cdot \nabla_{\Gamma_h} v ds_h \right. \\ &\quad + \int_{\Gamma_h} B^T (B^{-T} \nabla_{\Gamma_h} u^e) \cdot B^T (B^{-T} \nabla_{\Gamma_h} v) |B| ds_h \\ &\quad \left. - \int_{\Gamma_h} (B^{-T} \nabla_{\Gamma_h} u^e) \cdot (B^{-T} \nabla_{\Gamma_h} v) |B| ds_h \right| \\ &\lesssim \left(\|1 - |B|\|_{L^\infty(\Gamma_h)} + \|BB^T - I\|_{L^\infty(\Gamma_h)} \right) \|\nabla_{\Gamma} u\|_{L^2(\Gamma)} \|\nabla_{\Gamma_h} v\|_{L^2(\Gamma_h)} \\ &\lesssim h^{p+1} \|\nabla_{\Gamma} u\|_{L^2(\Gamma)} \|v\|_{a_h}. \end{aligned} \quad (8.17)$$

Term I_{II} . Changing the domain of integration we get

$$|l(v^l) - l_h(v)| = \left| \int_{\Gamma} f v^l ds - \int_{\Gamma_h} f_h v ds_h \right| \quad (8.18)$$

$$= \left| \int_{\Gamma_h} f^e v |B| ds_h - \int_{\Gamma_h} f_h v ds_h \right| \quad (8.19)$$

$$\lesssim \| |B| f^e - f_h \|_{L^2(\Gamma_h)} \|v\|_{L^2(\Gamma_h)} \quad (8.20)$$

$$\lesssim h^{p+1} \|f\|_{L^2(\Gamma)} \|v\|_{L^2(\Gamma)}, \quad (8.21)$$

where we at last used Assumption A3 on the data approximation f_h . Together, the bounds of I_I and I_{II} , and the Poincaré inequality (4.2), imply

$$I \lesssim h^{p+1} \|\nabla_{\Gamma} u\|_{L^2(\Gamma)} \|v\|_{a_h} + h^{p+1} \|f\|_{L^2(\Gamma)} \|v\|_{L^2(\Gamma_h)} \quad (8.22)$$

$$\lesssim (\|\nabla_{\Gamma} u\|_{L^2(\Gamma)} + \|f\|_{L^2(\Gamma)}) h^{p+1} \|v\|_{a_h}. \quad (8.23)$$

Finally, using that u is the solution of (2.5) we have the stability estimate $\|\nabla_{\Gamma} u\|_{L^2(\Gamma)} \lesssim \|f\|_{L^2(\Gamma)}$, and we obtain

$$I \lesssim h^{p+1} \|f\|_{L^2(\Gamma)} \|v\|_{a_h}. \quad (8.24)$$

Term II. Using the Cauchy-Schwarz inequality and Property P2 of the stabilization term, see Section 5, we obtain

$$|s_h(u^e, v)| \lesssim \|u^e\|_{s_h} \|v\|_{s_h} \lesssim h^p \|u\|_{H^{p+1}(\Gamma)} \|v\|_{s_h}. \quad (8.25)$$

Combining the estimates of I and II we obtain the desired estimate

$$|A_h(u^e, v) - l_h(v)| \lesssim h^p \|u\|_{H^{p+1}(\Gamma)} \|v\|_{A_h} + h^{p+1} \|f\|_{L^2(\Gamma)} \|v\|_{a_h}. \quad (8.26)$$

□

8.4 Error Estimates

We first prove optimal error estimates in the energy norm and then apply a duality argument to obtain L^2 -error estimates

Theorem 8.1 *Let $u \in H^{p+1}(\Gamma) \cap H_0^1(\Gamma)$ be the solution of (2.5) and $u_h \in V_h^p$ the finite element approximation defined by (3.3). If assumptions A1-A3 hold and the stabilization term has properties P1-P5 then, there is a constant independent of the mesh size h such that the following error bound holds*

$$\|u^e - u_h\|_{A_h} \lesssim h^p \|u\|_{H^{p+1}(\Gamma)} + h^{p+1} \|f\|_{L^2(\Gamma)}. \quad (8.27)$$

Proof. Using the Strang Lemma followed by the bounds on the interpolation error (8.8) and the consistency error (8.14) we get the desired bound. □

Theorem 8.2 *Let $u \in H^{p+1}(\Gamma) \cap H_0^1(\Gamma)$ be the solution of (2.5) and $u_h \in V_h^p$ the finite element approximation defined by (3.3). If assumptions A1-A3 hold and the stabilization term has properties P1-P5 then, there is a constant independent of the mesh size h such that the following error bound holds*

$$\|u^e - u_h\|_{L^2(\Gamma_h)} \lesssim h^{p+1} \|u\|_{H^{p+1}(\Gamma)} + h^{p+1} \|f\|_{L^2(\Gamma)}. \quad (8.28)$$

Proof. The proof is similar to the proof of the L^2 -error estimate in [3] for $p = 1$. Let

$e_h = u^e - u_h|_{\Gamma_h}$ and its lift on Γ be $e_h^l = u - u_h^l$. Recall that $\int_{\Gamma} u \, ds = 0$ and $\int_{\Gamma_h} u_h \, ds_h = 0$. We now define $\tilde{u}_h \in V_h^p$ as

$$\tilde{u}_h = u_h - |\Gamma|^{-1} \int_{\Gamma} u_h^l \, ds \quad (8.29)$$

so that we have $\int_{\Gamma} \tilde{u}_h^l = 0$. By adding and subtracting \tilde{u}_h^l and using the triangle inequality we obtain

$$\|e_h^l\|_{L^2(\Gamma)} \leq \underbrace{\|u - \tilde{u}_h^l\|_{L^2(\Gamma)}}_I + \underbrace{\|\tilde{u}_h^l - u_h^l\|_{L^2(\Gamma)}}_{II}. \quad (8.30)$$

Term I. Consider the dual problem:

$$a(v, \phi) = (\psi, v)_{\Gamma}, \quad \psi \in L^2(\Gamma) \setminus \mathbb{R}. \quad (8.31)$$

It follows from the Lax-Milgram lemma that there exists a unique solution in $H^1(\Gamma) \setminus \mathbb{R}$ and we also have the elliptic regularity estimate

$$\|\phi\|_{H^2(\Gamma)} \lesssim \|\psi\|_{L^2(\Gamma)}. \quad (8.32)$$

Setting $v = u - \tilde{u}_h^l$ in (8.31), adding and subtracting an interpolant, and using the weak formulations in (2.5) and (3.3) we obtain

$$(u - \tilde{u}_h^l, \psi)_{\Gamma} = a(u - \tilde{u}_h^l, \phi) \quad (8.33)$$

$$= a(u - \tilde{u}_h^l, \phi - (\pi_h^p \phi^e)^l) + a(u - \tilde{u}_h^l, (\pi_h^p \phi^e)^l) \quad (8.34)$$

$$= \underbrace{a(u - \tilde{u}_h^l, \phi - (\pi_h^p \phi^e)^l)}_{I_I} + \underbrace{l((\pi_h^p \phi^e)^l) - l_h(\pi_h^p \phi^e)}_{I_{II}} \quad (8.35)$$

$$+ \underbrace{a_h(\tilde{u}_h, \pi_h^p \phi^e) - a(\tilde{u}_h^l, (\pi_h^p \phi^e)^l)}_{I_{III}} + \underbrace{s_h(\tilde{u}_h, \pi_h^p \phi^e)}_{I_{IV}} \quad (8.36)$$

Term I_I. Using the Cauchy-Schwarz inequality, the norm equivalences (see Section 4), and the energy norm estimate (Theorem 8.1) we obtain

$$I_I \lesssim \|\nabla_{\Gamma}(u - \tilde{u}_h^l)\|_{L^2(\Gamma)} \|\nabla_{\Gamma}(\phi - (\pi_h^p \phi^e)^l)\|_{L^2(\Gamma)} \quad (8.37)$$

$$\lesssim \|u^e - u_h\|_{a_h} \|\phi^e - \pi_h^p \phi^e\|_{a_h} \quad (8.38)$$

$$\lesssim (h^p \|u\|_{H^{p+1}(\Gamma)} + h^{p+1} \|f\|_{L^2(\Gamma)}) \|\phi^e - \pi_h^p \phi^e\|_{a_h}. \quad (8.39)$$

The interpolation error estimate (8.10) with $s = 1$ yields

$$\|\phi^e - \pi_h^p \phi^e\|_{a_h} \lesssim h \|\phi\|_{H^2(\Gamma)} \quad (8.40)$$

and finally using the elliptic regularity estimate (8.32) we get

$$I_I \lesssim (h^{p+1} \|u\|_{H^{p+1}(\Gamma)} + h^{p+2} \|f\|_{L^2(\Gamma)}) \|\psi\|_{L^2(\Gamma)}. \quad (8.41)$$

Term $I_{II} - I_{III}$. We use the estimate of Term I in the proof of Lemma 8.3, together with the following stability estimate

$$\|\nabla_{\Gamma} \tilde{u}_h^l\|_{L^2(\Gamma)} = \|\nabla_{\Gamma} u_h^l\|_{L^2(\Gamma)} \lesssim \|u_h\|_{a_h} \lesssim \|f_h\|_{L^2(\Gamma_h)} \lesssim \|f\|_{L^2(\Gamma)} \quad (8.42)$$

to get

$$|I_{II} + I_{III}| \lesssim (h^{p+1} \|\nabla_{\Gamma} \tilde{u}_h^l\|_{L^2(\Gamma)} + h^{p+1} \|f\|_{L^2(\Gamma)}) \|\pi_h^p \phi^e\|_{a_h} \lesssim h^{p+1} \|f\|_{L^2(\Gamma)} \|\pi_h^p \phi^e\|_{a_h} \quad (8.43)$$

Adding and subtracting an interpolant, using the interpolation error estimate (8.40) followed by the elliptic regularity estimate (8.32) yield

$$\|\pi_h^p \phi^e\|_{a_h} \lesssim \|\pi_h^p \phi^e - \phi^e\|_{a_h} + \|\phi^e\|_{a_h} \lesssim \|\phi\|_{H^2(\Gamma)} \lesssim \|\psi\|_{L^2(\Gamma)}. \quad (8.44)$$

Thus,

$$|I_{II} + I_{III}| \lesssim h^{p+1} \|f\|_{L^2(\Gamma)} \|\psi\|_{L^2(\Gamma)}. \quad (8.45)$$

Term I_{IV} . We have

$$|I_{IV}| = |s_h(u_h, \pi_h^p \phi^e)| \lesssim \|u_h\|_{s_h} \|\pi_h^p \phi^e\|_{s_h}. \quad (8.46)$$

Using the energy norm error estimate, Theorem 8.1, and Property P2 of the stabilization we obtain

$$\|u_h\|_{s_h} \lesssim \|u_h - u^e\|_{s_h} + \|u^e\|_{s_h} \quad (8.47)$$

$$\lesssim h^p \|u\|_{H^{p+1}(\Gamma)} + h^{p+1} \|f\|_{L^2(\Gamma)} + h^p \|u\|_{H^{p+1}(\Gamma)} \quad (8.48)$$

and using Property P3 and the elliptic regularity estimate (8.32) we obtain

$$\|\pi_h^p \phi^e\|_{s_h} \lesssim h \|\phi\|_{H^2(\Gamma)} \lesssim h \|\psi\|_{L^2(\Gamma)}. \quad (8.49)$$

We thus have

$$|I_{IV}| \lesssim (h^{p+1} \|u\|_{H^{p+1}(\Gamma_h)} + h^{p+2} \|f\|_{L^2(\Gamma)}) \|\psi\|_{L^2(\Gamma)}. \quad (8.50)$$

Final Estimate of Term I . Collecting the estimates of Terms $I_I - I_{IV}$ and taking $\psi = u - \tilde{u}_h^l / \|u - \tilde{u}_h^l\|_{L^2(\Gamma)}$ we obtain

$$I = \|u - \tilde{u}_h^l\|_{L^2(\Gamma)} \lesssim h^{p+1} \|u\|_{H^{p+1}(\Gamma_h)} + h^{p+1} \|f\|_{L^2(\Gamma)}. \quad (8.51)$$

Term II . Using the definition (8.29) of \tilde{u}_h , adding $\int_{\Gamma_h} u_h ds_h = 0$, changing the domain of integration and using related bounds, employing the Poincaré inequality (4.2), and the stability estimate (8.42), we obtain

$$\|\tilde{u}_h^l - u_h^l\|_{L^2(\Gamma)} = \left| \int_{\Gamma} u_h^l ds - \int_{\Gamma_h} u_h ds_h \right| \quad (8.52)$$

$$\lesssim \left| \int_{\Gamma_h} u_h (|B| - 1) ds_h \right| \quad (8.53)$$

$$\lesssim h^{p+1} \|u_h\|_{L^2(\Gamma_h)} \quad (8.54)$$

$$\lesssim h^{p+1} \|u_h\|_{a_h} \quad (8.55)$$

$$\lesssim h^{p+1} \|f\|_{L^2(\Gamma)}. \quad (8.56)$$

Conclusion of the Proof. Using the estimates of Terms *I* and *II* in equation (8.30) and the equivalence $\|e_h^l\|_{L^2(\Gamma)} \sim \|e_h\|_{L^2(\Gamma_h)}$ conclude the proof. \square

9 Numerical Examples

We consider three different problems. The mesh on the domain where the interface is embedded is always generated independently of the position of the interface Γ and we use Lagrange basis functions.

9.1 The Laplace-Beltrami Problem

Let the interface Γ be a circle of radius 1 centered at the origin. We generate a uniform triangular mesh with $h = h_{x_1} = h_{x_2}$ on the computational domain: $[-1.5, 1.5] \times [-1.5, 1.5]$. A right-hand side f to equation (2.5) is calculated so that

$$u(x) = \frac{x_1^3 x_2^3}{(x_1^2 + x_2^2)^3} \quad (9.1)$$

is the exact solution. We discretize (2.5) using the proposed CutFEM with Lagrange basis functions of degree $p=1, 2$, and 3 .

In Fig. 4 we show the error and the spectral condition number of the linear systems as a function of the mesh size h . The error measured in the L^2 -norm behaves as $\mathcal{O}(h^{p+1})$ and in the H^1 -norm as $\mathcal{O}(h^p)$, as expected. The condition number behaves as $\mathcal{O}(h^{-2})$ independent of the polynomial degree and how the interface cuts the background mesh. The magnitude of the error and also the condition number depends on the stabilization constants in (3.8)-(3.9) and also on the choice of basis functions. For the results in Fig. 4 we have used $\gamma = 1$, $c_{F,j} = c_{\Gamma,j} = 2.5 \cdot 10^{-j}$, $j = 1, \dots, p$. We have not optimized this choice of parameters and other choices may give better results for example smaller condition numbers with almost the same error. We show this for example in Fig. 6 and 8. Other stabilization constants or basis functions can also give better scaling of the condition number with respect to the polynomial degree.

In Fig. 5 and 6 we show the effect of the stabilization on the error and the condition number for linear ($p=1$) and cubic elements ($p=3$), respectively. We show the convergence of the error with respect to the L^2 -norm. The results are similar when the error is measured in the H^1 -norm. We compare the proposed stabilization with the stabilization terms (1.8) and (1.10) and also show the condition number after diagonal scaling.

We see in Fig. 5 that for linear elements the errors, measured in the L^2 -norm, using the different stabilization terms and also no stabilization are very similar but we clearly see that when no stabilization is used the condition number can be extremely large depending on the position of the interface relative the background mesh. We have used $c_{F,1} = c_{\Gamma,1} = 10^{-1}$ and $\gamma = 1$ in the proposed stabilization. Note that the stabilization term (1.8) developed in [3] can be written in the form of the proposed stabilization, see (3.7)-(3.9), but with $c_{\Gamma,j} = 0$ for all j and $\gamma = 0$. For this stabilization we have chosen $c_{F,1} = 10^{-1}$ but since $\gamma = 0$ we get slightly larger errors than the other alternatives. Decreasing the stabilization constant $c_{F,1}$ will decrease the error. In the stabilization term (1.10) we have chosen $c_{\mathcal{T}} = 10^{-1}$ and $\alpha = 1$. We see in Fig. 5 that an alternative to adding stabilization terms is to do a simple diagonal scaling.

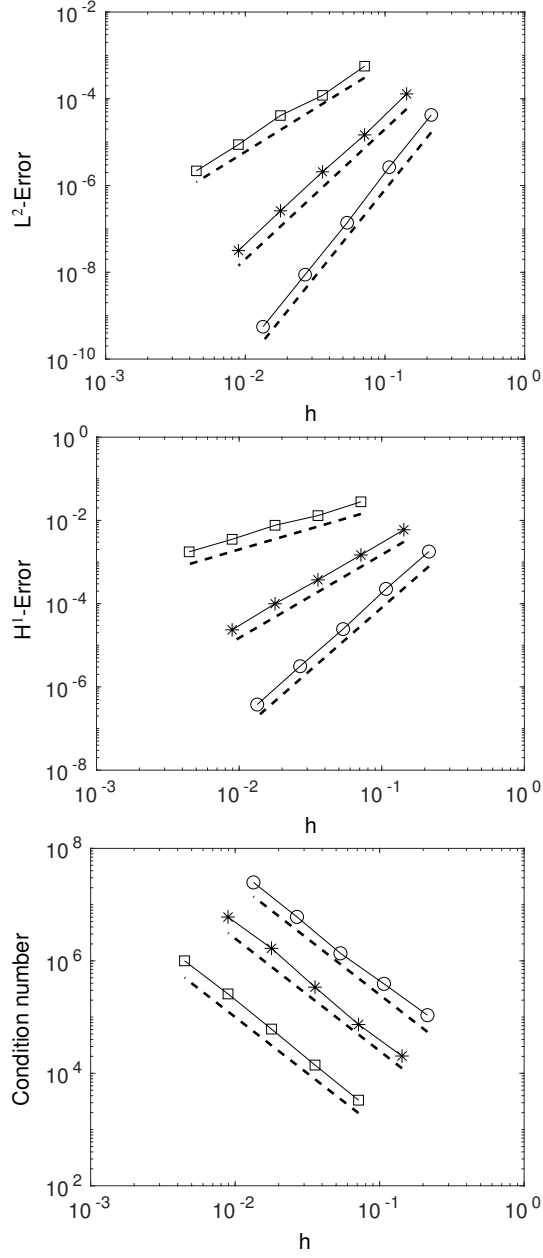


Figure 4: The Laplace-Beltrami problem: The error and condition number versus mesh size h for different degrees of polynomials, p , in the discretization. Squares: $p=1$. Stars: $p=2$. Circles: $p=3$. Top: The error measured in the L^2 -norm versus mesh size h . The dashed lines are indicating the expected rate of convergence and are proportional to h^{p+1} . Middle: The error measured in the H^1 -norm versus mesh size h . The dashed lines are indicating the expected rate of convergence and are proportional to h^p . Bottom: The condition number versus mesh size h . The dashed lines are all proportional to h^{-2} .

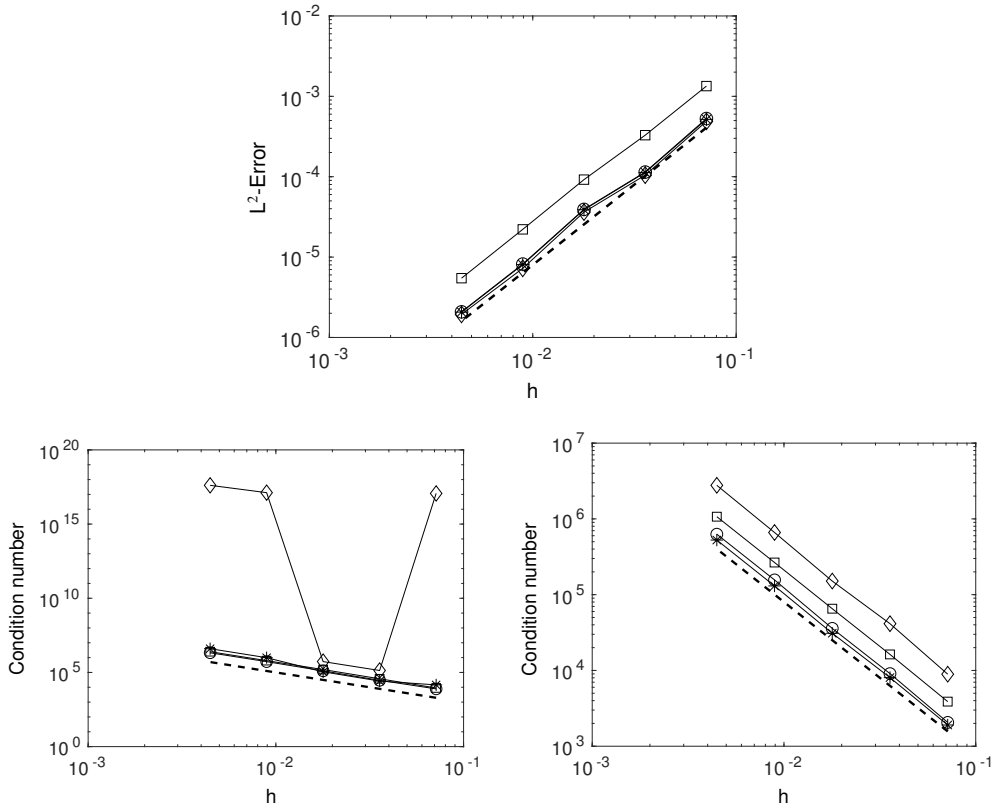


Figure 5: The Laplace-Beltrami problem: The error and condition number versus mesh size h using different stabilization terms. Linear elements are used, i.e. $p=1$. Diamonds: no stabilization is added. Circles: the proposed stabilization with $\gamma = 1$. Squares: the pure face stabilization (1.8). Stars: the normal gradient stabilization (1.10) with $\alpha = 1$. Top: The error measured in the L^2 -norm versus mesh size h . The dashed line is indicating the expected rate of convergence and is proportional to h^2 . Bottom left: The spectral condition number versus mesh size h . The dashed line is proportional to h^{-2} . Bottom right: The spectral condition number after diagonal scaling versus mesh size h . The dashed line is proportional to h^{-2} .

For higher order elements than linear the resulting linear systems from unstabilized Cut-FEM are severely ill-conditioned and neither a simple diagonal scaling alone or a pure face stabilization term such as (1.8) improves the condition number significantly, see Fig. 6. When the condition number becomes too large the convergence fails, the error is dominated by round-off errors and does not decrease with mesh refinement. In general, when the stabilization is not enough the behavior of the error depends on how the geometry cuts the background mesh. Therefore, if the approximation of the interface is slightly changed the magnitude of the error and the convergence shown in Fig. 6, where cubic elements are used, may change a lot for the unstabilized method and the method with only face stabilization. With the proposed stabilization and also with the stabilization term (1.10) we obtain as expected optimal convergence orders and the condition number of the linear systems scales as $\mathcal{O}(h^{-2})$ independent of how the interface cuts the background mesh. In Fig. 6 we also show results with different constants in the stabilization terms. We see that the magnitude of the error decreases as the stabilization term gets weaker. However, when the stabilization is too weak the condition number is large and roundoff errors dominate.

In Fig. 6 we see that the proposed stabilization and the stabilization term (1.10) resulted in very similar errors however the condition number is smaller when the stabilization term (1.10) is added to the weak form. The difference in the condition number decreases after a diagonal scaling of both matrices. We emphasize that all these results depend on the choice of parameters in the stabilization terms and the basis functions used. We have not optimized the parameters in the stabilization terms. For example, using cubic elements and the proposed stabilization term there are six constants and the parameter γ that one can modify to optimize the magnitude of the error and the condition number.

Next we vary both γ and the constants $c_{F,j}$ and $c_{\Gamma,j}$ in the proposed stabilization term and study the error and the condition number in Fig. 7 and 8 for linear and cubic elements, respectively. By decreasing the constants $c_{F,j}$ and $c_{\Gamma,j}$ and/or increasing γ we weaken the stabilization. In general, the error decreases while the condition number increases as the stabilization is weakened. The condition number also increases when the stabilization becomes too strong. We see this for the linear elements as well as the cubic elements. A strengthening of the stabilization sometimes decreases the condition number significantly but only increases the error slightly. Compare for example the black circles connected with a dashed dotted line, $\gamma = 0$ in Fig. 8 with the black circles connected with a solid line $\gamma = 1$ in the same figure. By lowering γ the error increases with a factor of 2.5 in this case but the condition number decreases with a factor 850. Comparing the results in Fig. 7 and 8 we see that the choice of parameters in the stabilization term have larger impact on the cubic elements than the linear elements. We also see that with other choices of parameters than the ones used for the results in Fig. 4 the condition number can scale much better with respect to the polynomial degree.

9.2 The Mass Matrix

We now consider the problem of finding $u_h \in V_h^p$ such that

$$\int_{\Gamma_h} u_h v_h \, ds_h + s_h(u_h, v_h) = \int_{\Gamma_h} f_h v_h \, ds_h, \quad (9.2)$$

where s_h is the stabilization term defined in (3.7). The interface Γ is a circle of radius 1 centered at the origin and we generate a uniform triangular mesh with $h = h_{x_1} = h_{x_2}$ on the

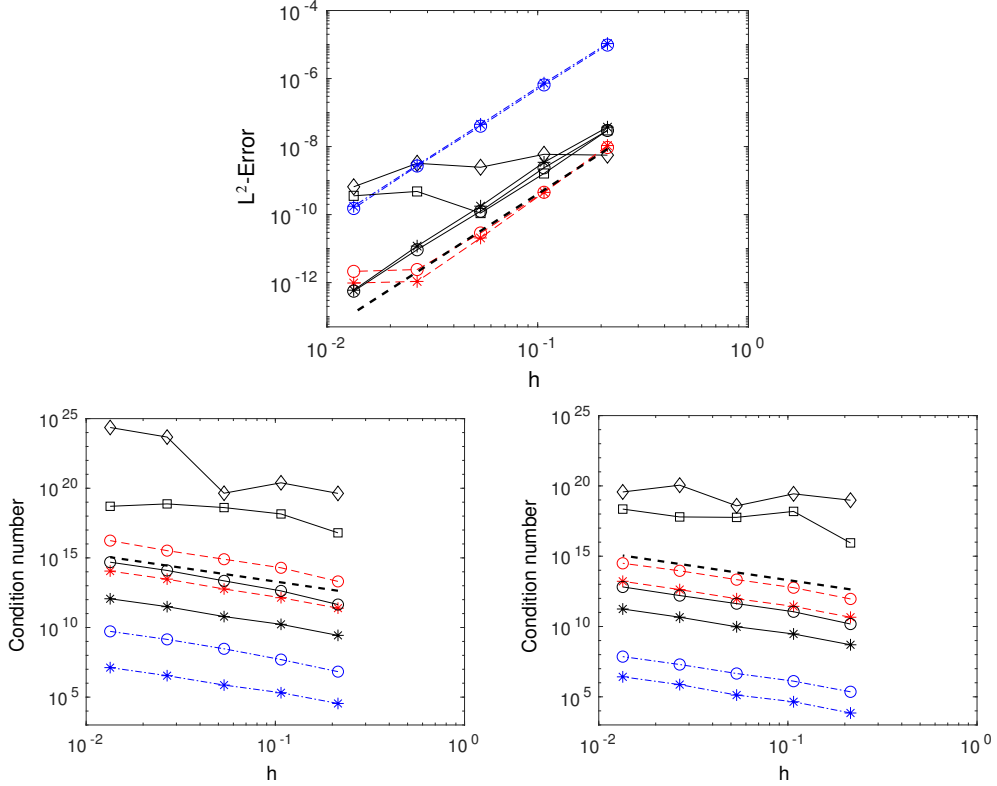


Figure 6: The Laplace-Beltrami problem: The error and condition number versus mesh size h using different stabilization terms. Cubic elements are used, i.e. $p=3$. Diamonds: no stabilization is added. Circles: the proposed stabilization with $\gamma = 1$. Squares: pure face stabilization. Stars: the stabilization term (1.10) with $\alpha = 1$. Top: The error measured in the L^2 -norm versus mesh size h . The dashed line is indicating the expected rate of convergence and is proportional to h^4 . Bottom left: The spectral condition number versus mesh size h . The dashed line is proportional to h^{-2} . Bottom right: The spectral condition number after diagonal scaling versus mesh size h . The dashed line is proportional to h^{-2} . Symbols connected with dashed dotted lines have larger constants in the stabilization terms than symbols connected with solid lines and symbols connected with dashed lines which have the smallest constants in the stabilization terms.

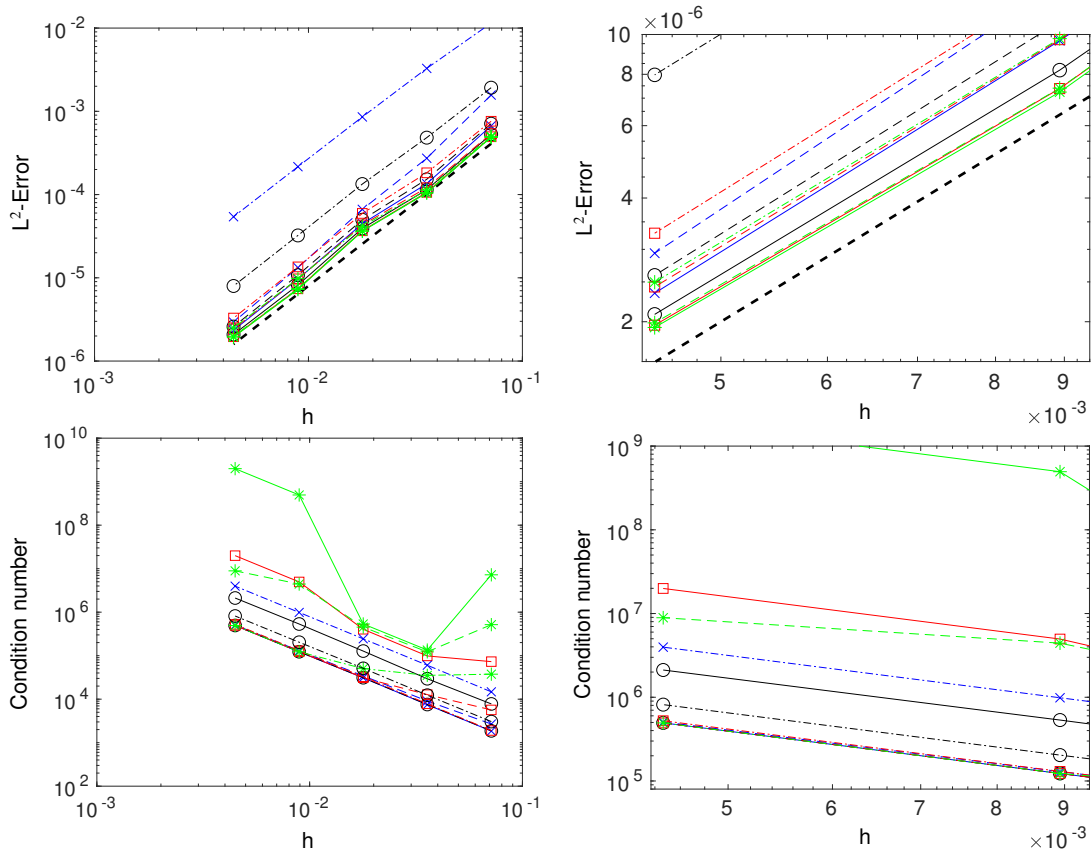


Figure 7: The Laplace-Beltrami problem: The error and the condition number versus mesh size h varying the stabilization constants and the parameter γ in (3.7)-(3.9). Linear elements are used, i.e. $p=1$. Solid lines: $\gamma = 1$. Dashed lines: $\gamma = 1/2$. Dashed dotted lines: $\gamma = 0$. $c_{F,1} = c_{\Gamma,1} = c$. Blue crosses: $c = 1$, Black circles: $c = 10^{-1}$. Red squares: $c = 10^{-2}$. Green stars: $c = 10^{-4}$. The figures to the right are close ups on part of the figures to the left so that the different curves can be distinguished.

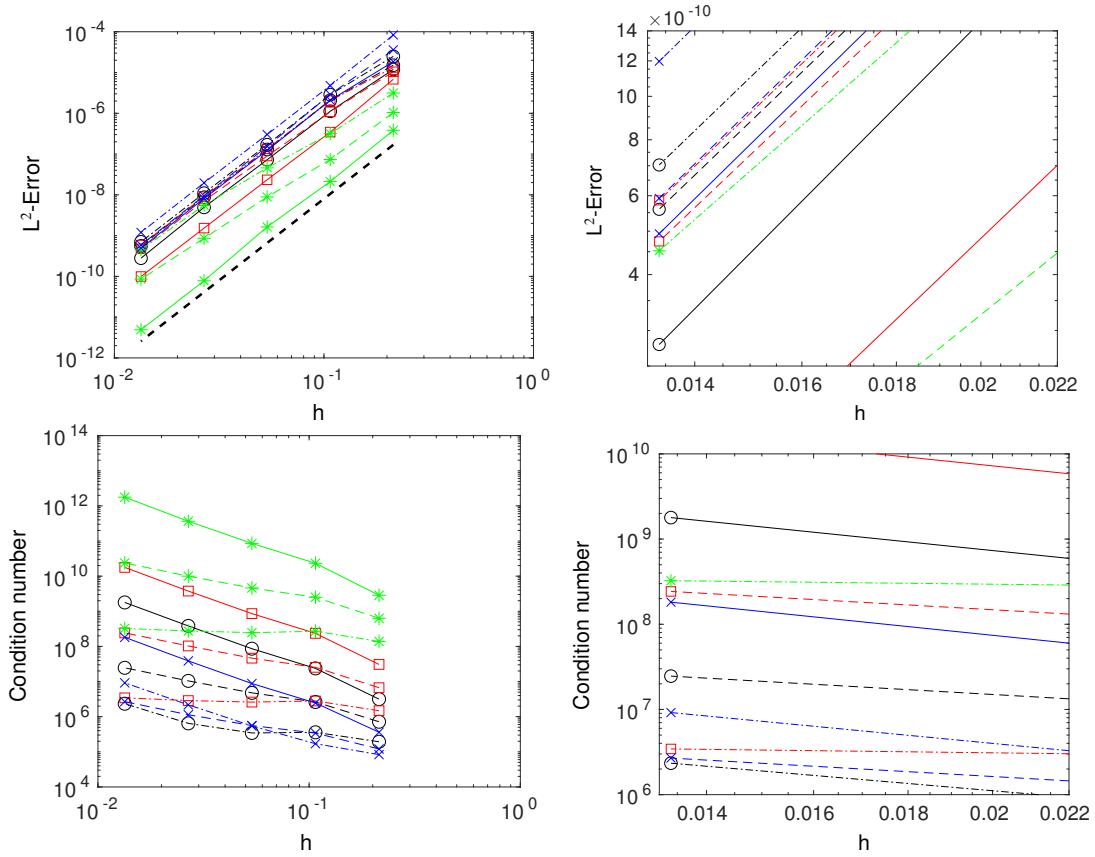


Figure 8: The Laplace-Beltrami problem: The error and the condition number versus mesh size h varying the stabilization constants and the parameter γ in (3.7)-(3.9). Cubic elements are used, i.e. $p=3$. Solid lines: $\gamma = 1$. Dashed lines: $\gamma = 1/2$. Dashed dotted lines: $\gamma = 0$. $c_{F,1} = c_{\Gamma,1} = c \cdot 0.07$, $c_{F,2} = c_{\Gamma,2} = c \cdot 0.004$, $c_{F,3} = c_{\Gamma,3} = c \cdot 2 \cdot 10^{-4}$. Blue crosses: $c = 1$. Black circles: $c = 10^{-1}$. Red squares: $c = 10^{-2}$. Green stars: $c = 10^{-4}$. The figures to the right are close ups on part of the figures to the left so that the different curves can be distinguished.

computational domain: $[-1.5, 1.5] \times [-1.5, 1.5]$. We let f_h be

$$f_h = \frac{-(6x_1x_2(x_1^4 - 4x_1^2x_2^2 + x_2^4))}{(x^2 + y^2)^4}. \quad (9.3)$$

We study the condition number of the mass matrix using different degrees of polynomials, p , and different stabilization terms. Fig. 9 shows that the stabilization term we propose results in optimal convergence rates in the L^2 -norm and optimal scaling of the condition number ($\mathcal{O}(1)$) of the mass matrix as it did for the Laplace-Beltrami operator. As before, the parameters used in (3.7)-(3.9) influence the magnitude of the error and the condition number. For the results shown in Fig. 9 we have used $c_{F,j} = c_{\Gamma,j} = 0.03 \cdot 20^{-j}$, $j = 1, \dots, p$. Other choices could give smaller condition numbers without increasing the error significantly and also give better scaling with respect to the polynomial degree of the condition number.

In Fig. 10 and 11 we compare different stabilization terms for linear and cubic elements, respectively. The proposed stabilization with $\gamma = 1$ is compared with using no stabilization i.e., $c_{F,j} = c_{\Gamma,j} = 0$, a pure face stabilization i.e. $c_{\Gamma,j} = 0$ with $\gamma = 1$, a pure interface stabilization i.e. $c_{F,j} = 0$ with $\gamma = 1$, and the stabilization term (1.10) with $\alpha = 1$. In Fig. 10 we also show results with two different constants in the stabilization terms. We see that only the proposed stabilization and the stabilization term (1.10) yield optimal scaling of the condition number ($\mathcal{O}(1)$) and both the error and the condition number are very similar for these two stabilization terms.

For cubic elements we show results with three different constants in the stabilization terms, see Fig. 11. Decreasing the constants in the stabilization decreases the magnitude of the error but the condition number increases. When the stabilization is too weak the convergence rate is not optimal.

Our observations are similar to what we observed for the Laplace-Beltrami operator. For higher order elements the linear systems are severely ill-conditioned without stabilization and the behavior of the error is oscillatory and the convergence rate will depend on how the geometry cuts the background mesh. We also see that neither the pure face stabilization nor a pure interface stabilization give enough control of the condition number and that we need, as we propose, the combination of them.

9.3 The Mean Curvature Vector

We consider the interfaces given by the zero contour of the following level set functions

$$\phi = \frac{x^2}{0.64} + y^2 - 0.25 \quad \text{Ellipse} \quad (9.4)$$

$$\phi = \left(z^2 + \left((x^2 + y^2)^{1/2} - 1 \right)^2 \right)^{1/2} - 0.5 \quad \text{Torus} \quad (9.5)$$

$$\phi = 0.02 - ((x^2 + y^2 - 0.75)^2 + (z^2 - 1)^2)((y^2 + z^2 - 0.75)^2 + (x^2 - 1)^2) \quad \text{Deco-cube} \quad (9.6)$$

$$(9.7)$$

We generated meshes independently of the position of the given interface. We define the mesh size by $h = 1/N^{\frac{1}{d}}$ where N denotes the total number of nodes. We construct an approximate level set function ϕ_h using the nodal interpolant $\pi_h^1 \phi$ on the background mesh and let the

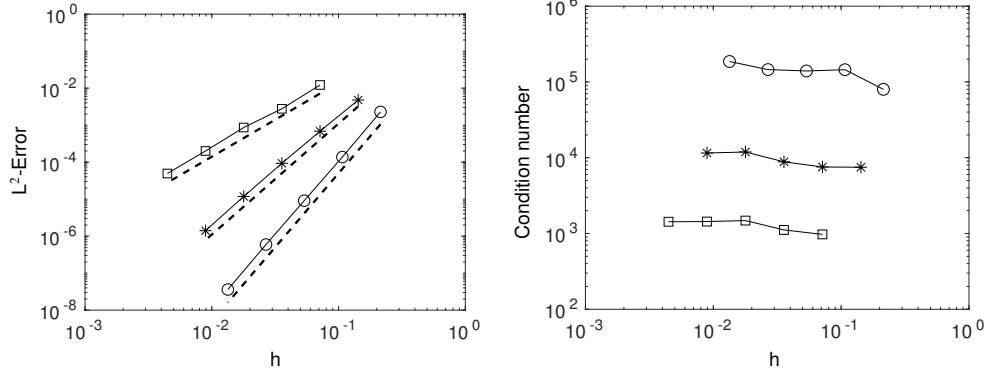


Figure 9: The mass matrix: The error and condition number versus mesh size h for different degrees of polynomials, p , in the space discretization. Squares: $p=1$. Stars: $p=2$. Circles: $p=3$. Left: The error measured in the L^2 -norm versus mesh size h . The dashed lines are indicating the expected rate of convergence and are proportional to h^{p+1} . Right: The condition number versus mesh size h .

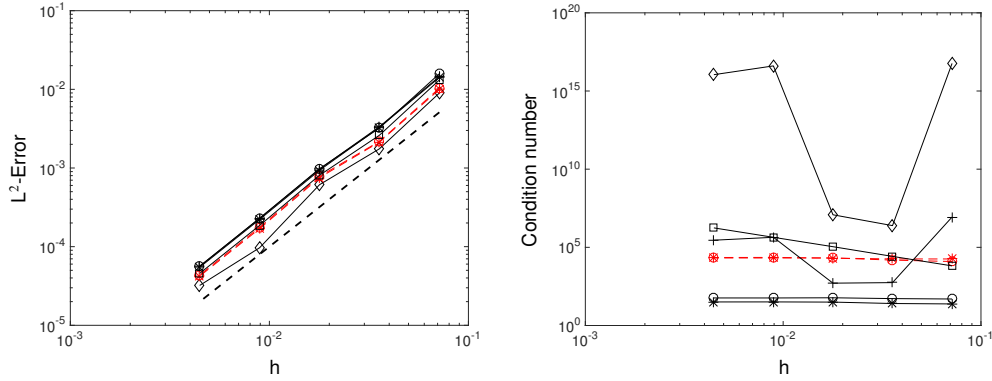


Figure 10: The mass matrix: The error and condition number versus mesh size h using different stabilization terms. Linear elements are used, i.e. $p=1$. Diamonds: no stabilization is added. Circles: the proposed stabilization with $\gamma = 1$. Squares: the pure face stabilization. Stars: the stabilization term (1.10) with $\alpha = 1$. Left: The error measured in the L^2 -norm versus mesh size h . The dashed line is indicating the expected rate of convergence and is proportional to h^2 . Right: The condition number versus mesh size h . Symbols connected with solid lines: $c_{F,j} = 10^{-1}$, $c_{\Gamma,j} = 10^{-1}$ and $c_{\mathcal{T}} = 10^{-1}$ in (1.10). Symbols connected with dashed lines: $c_{F,j} = c_{\Gamma,j} = 10^{-4}$, and $c_{\mathcal{T}} = 10^{-4}$.

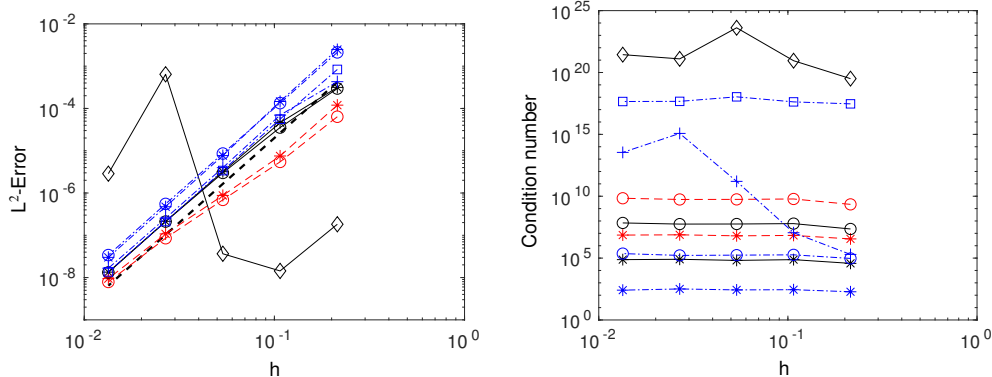


Figure 11: The mass matrix: The error and condition number versus mesh size h using different stabilization parameters. Cubic elements are used, i.e. $p=3$. Diamonds: no stabilization is added. Circles: the proposed stabilization with $\gamma = 1$. Squares: the pure face stabilization. Stars: the stabilization term (1.10) with $\alpha = 1$. Left: The error measured in the L^2 -norm versus mesh size h . The dashed line is indicating the expected rate of convergence and is proportional to h^4 . Right: The condition number versus mesh size h . Symbols connected with dashed dotted lines (blue) have larger constants in the stabilization terms than symbols connected with solid lines (black) and symbols connected with dashed lines (red) which have the smallest constants in the stabilization terms.

interface be the zero level set of ϕ_h . We use linear Lagrange basis functions. Given the discrete coordinate map $x_{\Gamma_h} : \Gamma_h \ni x \mapsto x \in \mathbf{R}^d$ we want to find the stabilized discrete mean curvature vector $H_h \in [V_h^1]^d$ such that

$$(H_h, v_h)_{\Gamma_h} + s_h(H_h, v_h) = (\nabla_{\Gamma_h} x_{\Gamma_h}, \nabla_{\Gamma_h} v_h)_{\Gamma_h}, \quad (9.8)$$

where s_h is a stabilization term. The torus and the deco-cube are examples from [22]. In [22] we proved that using the ghost penalty stabilization (1.8) the method (9.8) is a convergent first order method with respect to the L^2 -norm. Therefore, we also expect to obtain first order accurate approximations of the mean curvature vector using the proposed stabilization term.

We compare the approximation from (9.8) with the vector $H = -(\nabla \cdot n)n$, where $n = \frac{\nabla \phi}{|\nabla \phi|}$. In Fig. 12 we show the error in the L^2 -norm using the proposed stabilization with $\gamma = 0$ and the stabilization term (1.10) developed in [5] and [18] with $\alpha = -1$. We emphasize that the analysis in [22] requires control over the jumps in the normal derivatives across edges on Γ_h , which can be controlled using (1.8), and without appropriate stabilization we don't expect any convergence in L^2 . Note also that we do not expect the element normal gradient stabilization to provide enough stabilization to ensure convergence of the mean curvature vector since some additional tangential control is required and thus this is a situation where face stabilization comes in naturally. In practice, we note that depending on the stabilization parameter we see that we are able to obtain first order convergence with both stabilization terms. However, the magnitude of the errors are always smaller using the proposed stabilization compared to using the stabilization term (1.10). The magnitude of the error using the pure face stabilization is similar to the results with the proposed stabilization and not shown here. Furthermore, the condition number is better using the proposed stabilization term. We emphasize that when higher order elements than linear are used it is of vital importance to use the proposed

stabilization term to control the condition number since the pure face stabilization does not control the condition number and therefore the error may be dominated by roundoff errors. Full details of high order approximations of the mean curvature vector using this approach are presented in [16].

In this example the face stabilization is of importance and in such cases the proposed stabilization is preferable compared to the stabilization term (1.10).

10 Discussion

A strategy to control the condition number of the system matrix resulting from cut finite element discretizations, independently of how elements in the background mesh are cut by the geometry, is to add a stabilization term to the weak formulation. For higher order elements than linear the linear systems resulting from cut finite element discretizations without stabilization are extremely ill-conditioned and it is not obvious how to precondition such linear systems. Therefore, the strategy of adding a stabilization term to the weak form has become a popular alternative to cure this ill-conditioning. The stabilization term most frequently used together with CutFEM is the ghost penalty stabilization [10] which acts only on the element faces. We have seen in this work that when higher order elements than linear are used in the cut finite element discretizations of surface PDEs the condition number can not be controlled by only adding such a face stabilization term. We have proposed a remedy where we keep the face stabilization but also add a stabilization term acting on the interface/surface and prove that this new stabilization term controls the condition number for both linear as well as higher order elements.

As discussed in the introduction and in Section 9 a different stabilization term, the normal gradient stabilization (1.10) which is evaluated on each cut element, has recently been proposed in [5] and [18]. For surface PDEs this stabilization also controls the condition number for linear as well as higher order elements. This term results in less non-zero entries in the stiffness matrix than the stabilization term we propose since it is local while the face stabilization term involves neighboring elements. The implementation of (1.10) is also easier than the stabilization we propose. However, there are a couple of reasons why we choose to keep the ghost penalty term and propose a stabilization term based on this term.

- The element stabilization (1.10) cannot be used in the discretization of bulk problems since it would destroy the convergence order while the ghost penalty stabilization could be used without destroying the convergence order and with control of the condition number of the linear systems. Many applications include coupled bulk-surface problems and for those problems the ghost penalty stabilization is needed. In such applications, the effect of the proposed stabilization on the number of non-zero elements is very small and since the face stabilization is needed for the bulk problem the implementation of the proposed stabilization is also easy as only the stabilization term acting on the surface has to be added.
- The ghost penalty stabilization has shown to be of importance also for other reasons than controlling the condition number. In [9], for example, we show that by adding such a face stabilization we get a stable discretization for convection dominated problems on surfaces and no other stabilization term such as for example a SUPG term is needed. In [22] we show that with the same face stabilization a method for computing the mean curvature

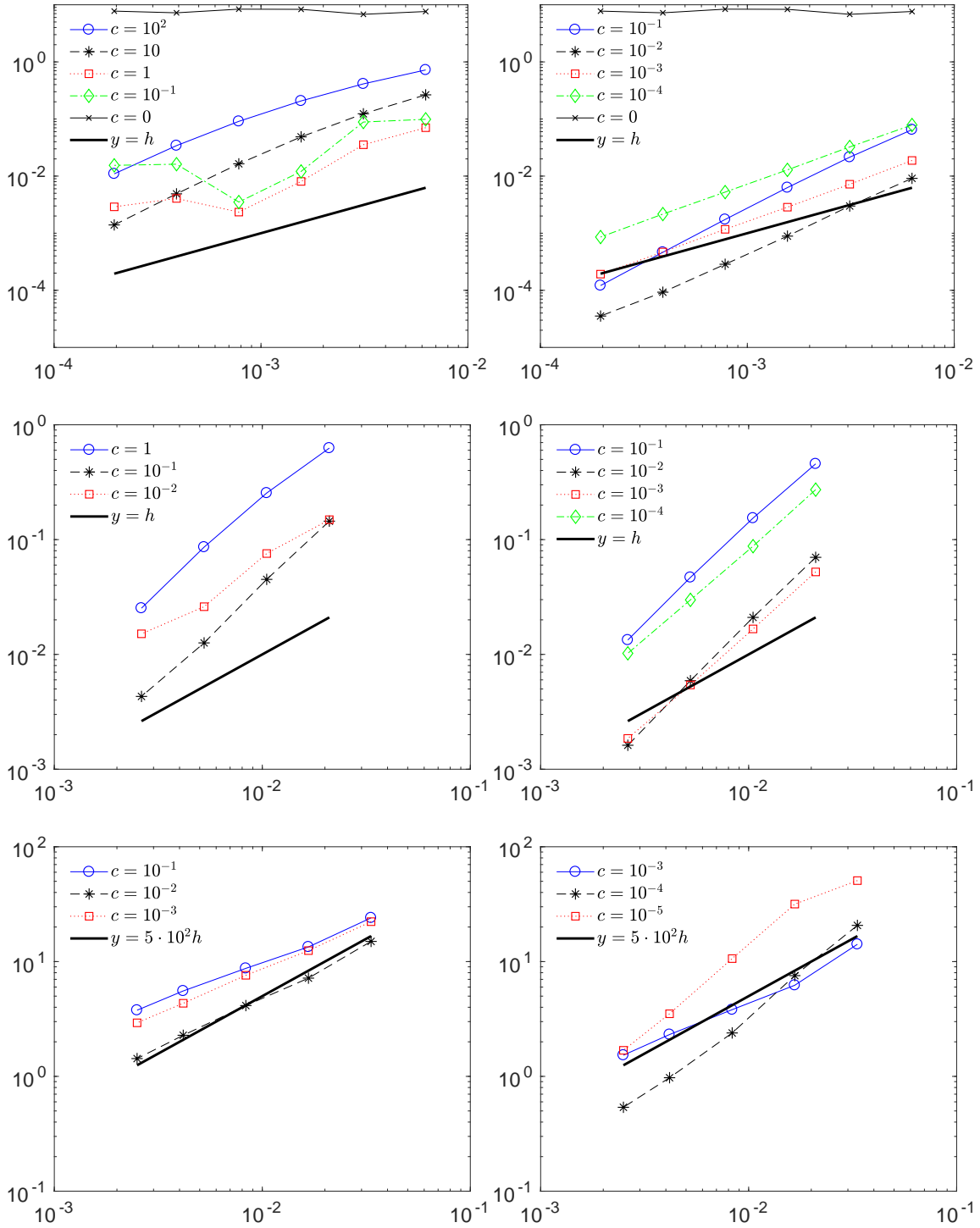


Figure 12: The mean curvature vector: The error measured in the L^2 -norm versus mesh size h . Linear elements are used, i.e. $p=1$. Left: The stabilization term (1.10) developed in [5] and [18] with $\alpha = -1$ and $c_{\mathcal{T}} = c$. Right: The proposed stabilization with $\gamma = 0$ and $c_F = c_{\Gamma} = c$. Top: Ellipse. Middle: Torus. Bottom: Deco-cube.

vector for piecewise linear surfaces based on the Laplace–Beltrami operator enjoys first order convergence in the L^2 -norm while, in general, without the stabilization convergence cannot be expected. In Section 9.3 we compute the mean curvature vector of three surfaces and show that we obtain better accuracy with the proposed stabilization than with the stabilization (1.10). Our method for computing the mean curvature vector can also be extended to give high order approximations [16]. For time dependent problems on surfaces and coupled-bulk surface problems adding the ghost penalty stabilization enables to directly approximate space-time integrals in space-time cut finite element formulations using quadrature rules for the integrals over time [23, 30]. This makes the implementation of space-time CutFEM convenient when higher order elements are used, in particular for coupled bulk-surface problems. The proposed stabilization thus also has all these advantages and in addition gives control of the condition number for linear as well as higher order elements.

- The proof of the condition number estimate is simple when the proposed stabilization term is used. The main step in the proof is to show that one covers a non empty set inside an element by going in the normal direction of the surface from the part of the surface that intersects the element. For the proposed stabilization one only needs to show that such a non-empty set exist for elements that have a large intersection with the surface. However, to obtain the desired Poincaré inequality with the stabilization term (1.10) one needs to show that such a set exist in each element and in particular that this set is large enough [5, 18]. We use the simplified structure of the proof to extend our results to the case of general codimension embeddings, see Section 7 where we present the minor modifications of the proof to Lemma 6.3 to verify the generalized version (7.4) of the Poincaré inequality P5.
- We also note that the stabilization term (1.10) requires the computation of the normal vector inside an element. When the interface is implicitly represented by a higher dimensional function, for example a distance function, this normal vector can be taken to be the normal vector of the level sets of the function defining the interface implicitly. However, when an explicit representation is used for the surface a normal vector inside an element is not immediately available but normal vectors on the surface, used in the proposed stabilization, are available.

References

- [1] S. C. Brenner and L. R. Scott. *The Mathematical Theory of Finite Element Methods*. Springer-Verlag, 2008.
- [2] E. Burman, S. Claus, P. Hansbo, M. G. Larson, and A. Massing. CutFEM: discretizing geometry and partial differential equations. *Internat. J. Numer. Methods Engrg.*, 104(7):472–501, 2015.
- [3] E. Burman, P. Hansbo, and M. G. Larson. A stabilized cut finite element method for partial differential equations on surfaces: the Laplace-Beltrami operator. *Comput. Methods Appl. Mech. Engrg.*, 285:188–207, 2015.
- [4] E. Burman, P. Hansbo, M. G. Larson, and K. Larsson. Cut Finite Elements for Convection in Fractured Domains. *ArXiv e-prints*, January 2018.

- [5] E. Burman, P. Hansbo, M. G. Larson, and A. Massing. Cut finite element methods for partial differential equations on embedded manifolds of arbitrary codimensions. *ArXiv e-prints*, October 2016.
- [6] E. Burman, P. Hansbo, M. G. Larson, and A. Massing. A cut discontinuous Galerkin method for the Laplace-Beltrami operator. *IMA J. Numer. Anal.*, 37(1):138–169, 2017.
- [7] E. Burman, P. Hansbo, M. G. Larson, A. Massing, and S. Zahedi. Full gradient stabilized cut finite element methods for surface partial differential equations. *Comput. Methods Appl. Mech. Engrg.*, 310:278–296, 2016.
- [8] E. Burman, P. Hansbo, M. G. Larson, and S. Zahedi. Cut finite element methods for coupled bulk-surface problems. *Numer. Math.*, 133(2):203–231, 2016.
- [9] E. Burman, P. Hansbo, M. G. Larson, and S. Zahedi. Stabilized cutfem for the convection problem on surfaces. *Accepted for publication in Numer. Math.*, 2018.
- [10] Erik Burman. Ghost penalty. *C. R. Acad. Sci. Paris, Ser. I*, 348(21-22):1217 – 1220, 2010.
- [11] M. Cenanovic, P. Hansbo, and M. G. Larson. Minimal surface computation using a finite element method on an embedded surface. *Internat. J. Numer. Methods Engrg.*, 104(7):502–512, 2015.
- [12] M. Cenanovic, P. Hansbo, and M. G. Larson. Cut finite element modeling of linear membranes. *Comput. Methods Appl. Mech. Engrg.*, 310:98–111, 2016.
- [13] K. Deckelnick, C. M. Elliott, and T. Ranner. Unfitted finite element methods using bulk meshes for surface partial differential equations. *SIAM J. Numer. Anal.*, 52(4):2137–2162, 2014.
- [14] A. Demlow and G. Dziuk. An adaptive finite element method for the Laplace-Beltrami operator on implicitly defined surfaces. *SIAM J. Numer. Anal.*, 45(1):421–442 (electronic), 2007.
- [15] A. Demlow and M. A. Olshanskii. An adaptive surface finite element method based on volume meshes. *SIAM J. Numer. Anal.*, 50(3):1624–1647, 2012.
- [16] T. Frachon and S. Zahedi. High order stabilized finite element approximations of the mean curvature vector. Technical report, Mathematics, KTH, Sweden, 2018.
- [17] D. Gilbarg and N. S. Trudinger. *Elliptic partial differential equations of second order*. Classics in Mathematics. Springer-Verlag, Berlin, 2001. Reprint of the 1998 edition.
- [18] J. Grande, C. Lehrenfeld, and A. Reusken. Analysis of a high order trace finite element method for pdes on level set surfaces. *ArXiv e-prints*, November 2016.
- [19] S. Gross, M. A. Olshanskii, and A. Reusken. A trace finite element method for a class of coupled bulk-interface transport problems. *ESAIM Math. Model. Numer. Anal.*, 49(5):1303–1330, 2015.
- [20] A. Hansbo, P. Hansbo, and M. G. Larson. A finite element method on composite grids based on Nitsche’s method. *M2AN Math. Model. Numer. Anal.*, 37(3):495–514, 2003.

- [21] P. Hansbo, M. G. Larson, and K. Larsson. Cut finite element methods for linear elasticity problems. *ArXiv e-prints*, March 2017.
- [22] P. Hansbo, M. G. Larson, and S. Zahedi. Stabilized finite element approximation of the mean curvature vector on closed surfaces. *SIAM J. Numer. Anal.*, 53(4):1806–1832, 2015.
- [23] P. Hansbo, M. G. Larson, and S. Zahedi. A cut finite element method for coupled bulk-surface problems on time-dependent domains. *Comput. Methods Appl. Mech. Engrg.*, 307:96–116, 2016.
- [24] M. A. Olshanskii and A. Reusken. A finite element method for surface PDEs: matrix properties. *Numer. Math.*, 114(3):491–520, 2010.
- [25] M. A. Olshanskii and A. Reusken. Error analysis of a space-time finite element method for solving PDEs on evolving surfaces. *SIAM J. Numer. Anal.*, 52(4):2092–2120, 2014.
- [26] M. A. Olshanskii, A. Reusken, and J. Grande. A finite element method for elliptic equations on surfaces. *SIAM J. Numer. Anal.*, 47(5):3339–3358, 2009.
- [27] M. A. Olshanskii, A. Reusken, and X. Xu. An Eulerian space-time finite element method for diffusion problems on evolving surfaces. *SIAM J. Numer. Anal.*, 52(3):1354–1377, 2014.
- [28] M. A. Olshanskii, A. Reusken, and X. Xu. A stabilized finite element method for advection-diffusion equations on surfaces. *IMA J. Numer. Anal.*, 34(2):732–758, 2014.
- [29] A. Reusken. Analysis of trace finite element methods for surface partial differential equations. *IMA J. Numer. Anal.*, 35(4):1568–1590, 2015.
- [30] S. Zahedi. A space-time cut finite element method with quadrature in time. In *Geometrically Unfitted Finite Element Methods and Applications*, Lecture Notes in Computational Science and Engineering. Springer, 2018.